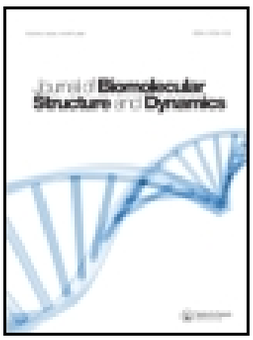

Taylor & Francis
Taylor & Francis Group

Journal of Biomolecular Structure and Dynamics

ISSN: (Print) (Online) Journal homepage: https://www.tandfonline.com/loi/tbsd20

Carbazole-based semicarbazones and hydrazones as multifunctional anti-Alzheimer agents

Kishan B. Patel, Dushyant V. Patel, Nirav R. Patel, Ashish M. Kanhed, Divya M. Teli, Bhumi Gandhi, Bhavik S. Shah, Bharat N. Chaudhary, Navnit K. Prajapati, Kirti V. Patel & Mange Ram Yadav

To cite this article: Kishan B. Patel, Dushyant V. Patel, Nirav R. Patel, Ashish M. Kanhed, Divya M. Teli, Bhumi Gandhi, Bhavik S. Shah, Bharat N. Chaudhary, Navnit K. Prajapati, Kirti V. Patel & Mange Ram Yadav (2021): Carbazole-based semicarbazones and hydrazones as multifunctional anti-Alzheimer agents, Journal of Biomolecular Structure and Dynamics, DOI: 10.1080/07391102.2021.1942212

To link to this article: https://doi.org/10.1080/07391102.2021.1942212

View supplementary material

Published online: 02 Jul 2021.

Submit your article to this journal

Article views: 30

View related articles

View Crossmark data

Full Terms & Conditions of access and use can be found at
https://www.tandfonline.com/action/journalInformation?journalCode=tbsd20

JOURNAL OF BIOMOLECULAR STRUCTURE AND DYNAMICS
https://doi.org/10.1080/07391102.2021.1942212

Taylor & Francis
Taylor & Francis Group

Check for updates

Carbazole-based semicarbazones and hydrazones as multifunctional anti-Alzheimer agents

Kishan B. Patel[a], Dushyant V. Patel[a], Nirav R. Patel[a], Ashish M. Kanhed[b], Divya M. Teli[c], Bhumi Gandhi[a], Bhavik S. Shah[a], Bharat N. Chaudhary[a], Navnit K. Prajapati[a], Kirti V. Patel[a] and Mange Ram Yadav[a,d]

[a]Faculty of Pharmacy, The Maharaja Sayajirao University of Baroda, Vadodara, Gujarat, India; [b]Shobhaben Pratapbhai Patel – School of Pharmacy & Technology Management, SVKM's NMIMS University, Mumbai, India; [c]Department of Pharmaceutical Chemistry, L. M. College of Pharmacy, Navrangpura, Gujarat, India; [d]Centre of Research for Development, Parul University, Vadodara, Gujarat, India

Communicated by Ramaswamy H. Sarma

ABSTRACT

With the aim to combat a multi-faceted neurodegenerative Alzheimer's disease (AD), a series of carbazole-based semicarbazide and hydrazide derivatives were designed, synthesized and assessed for their cholinesterase (ChE) inhibitory, antioxidant and biometal chelating activity. Among them, (*E*)-2-((9-ethyl-9*H*-carbazol-3-yl)methylene)-*N*-(pyridin-2-yl)hydrazinecarbothioamide (**62**) and (*E*)-2-((9-ethyl-9*H*-carbazol-3-yl)methylene)-*N*-(5-chloropyridin-2-yl)hydrazinecarbothioamide (**63**) emerged as the premier candidates with good ChE inhibitory activities (IC_{50} values of 1.37 μM and 1.18 μM for *h*AChE, IC_{50} values of 2.69 μM and 3.31 μM for *Eq*BuChE, respectively). All the test compounds displayed excellent antioxidant activity (reduction percentage of DPPH values for compounds (**62**) and (**63**) were 85.67% and 84.49%, respectively at 100 μM concentration). Compounds (**62**) and (**63**) conferred specific copper ion chelating property in metal chelation study. Molecular docking studies of compounds (**62**) and (**63**) indicate strong interactions within the active sites of both the ChE enzymes. Besides that, these compounds also exhibited significant *in silico* drug-like pharmacokinetic properties. Thus, taken together, they can serve as a starting point in the designing of multifunctional ligands in pursuit of potential anti-AD agents that might further prevent the progression of ADs.

ARTICLE HISTORY
Received 22 December 2020
Accepted 7 June 2021

KEYWORDS
Acetylcholinesterase; butyrylcholinesterase; metal chelation; MTDL; carbazole; Alzheimer's disease

1. Introduction

Alzheimer's disease (AD) is a neurodegenerative disease, causing severe neuronal disruption in the hippocampus and cerebral cortex regions of the brain. This is recognized by impairment of the cognitive functions, usually leading to deterioration in emotional control, social behavior or motivation (Goedert & Spillantini, 2006). Globally, over 50 million people are currently affected by AD and the toll is expected to rise upto 150 million by 2050 (Patel, Patel, Kanhed, Teli, Patel, Gandhi, et al., 2020; World Alzheimer Report, 2019).

The neuropathological hallmarks of the AD brain are low levels of acetylcholine (ACh) (Talesa, 2001), diffused extracellular amyloid plaques caused by self or biometal-mediated β-amyloid (Aβ) aggregation, which are frequently surrounded by damaged neurons (Selkoe, 2003), and hyperphosphorylated intracellular neurofibrillary tangles (Maccioni et al., 2010). These well-recognized pathological hallmarks are often accompanied by high levels of oxidative stress generated by reactive oxygen species (ROS) and biometal dyshomeostasis (Greenough et al., 2013). Therefore, to combat a multifactorial disease like AD, development of multi-target-directed ligands (MTDLs) is considered a promising drug discovery approach (Bajda et al., 2011; Oset-Gasque & Marco-Contelles, 2018; Patel et al., 2019; Wang et al., 2019). Currently, there are only four FDA-approved medications available to treat AD, of which three are acetylcholinesterase (AChE) inhibitors (donepezil, galantamine and rivastigmine) and the fourth one is *N*-methyl-D-aspartate (NMDA) receptor antagonist (memantine). These drugs can relieve the symptoms of AD, but they are not able to reverse the progression of the illness.

Deficits in the cholinergic neurons and transmission located in the basal forebrain could severely affect many facets of cognition and behavior, including cortical and hippocampal memory processing. The low levels of ACh are due to its excessive hydrolysis by cholinesterases (ChEs) present in the brain. Therefore, inhibition of ChEs is considered to be an effective strategy to increase ACh levels within the brain (Greig et al., 2002; Hartmann et al., 2007; Jing et al., 2019). Recent studies have indicated that AChE could play a key role in deposition of amyloid plaques. However, in later stages of AD, diminished levels of AChE and upsurged or unaltered levels of BuChE have been reported (Holzgrabe et al., 2007). This suggests that if AD patients are treated with dual AChE and BuChE inhibitors it may lead to more assured results.

Under normal physiological conditions, the production of ROS and reactive nitrogen species (RNS) is counter balanced

CONTACT Mange Ram Yadav mryadav11@yahoo.co.in
Supplemental data for this article can be accessed online at https://doi.org/10.1080/07391102.2021.1942212.
© 2021 Informa UK Limited, trading as Taylor & Francis Group

by the antioxidant activities of various defensive mechanisms that include several antioxidants and enzymes. The imbalance between the ROS generation or reduction in its metabolic destruction will shift the equilibrium of the cellular redox balance to an oxidative imbalance, leading thereby to the overproduction of ROS (Poljuha et al., 2015). The change in the redox transition metal balance, particularly of copper, iron and zinc ions are crucial. Binding of these metal ions to Aβ causes dyshomeostasis that leads to an apparent state of Cu deficiency in the intracellular region and an extracellular rise in Cu and Zn levels. The metal dyshomeostasis causes production of oxidative stress by dysfunction of various important cuproenzymes and antioxidants such as superoxide dismutase 1 (SOD1) resulting in the dysfunction of neuronal cells, which in turn reduces the synaptic transmission.

Based on these reports and extending our ongoing research work, we report herein designing, synthesis and biological evaluation (ChE inhibition, antioxidant and metal chelation studies) of a series of novel carbazole-based substituted thiosemicarbazide and hydrazide derivatives as potential anti-AD agents. The binding modes and interactions of the compounds with the target proteins were determined by performing molecular docking and molecular dynamics simulation studies. The most promising compounds were then screened *in silico* for their virtual ADMET properties.

2. Rationale of designing

The mono-targeted anti-AD agents, even though having high binding affinity and selectivity for a specific target, might not be that much effective to combat AD having a complex etiology. In contrast to a mono-targeted ligand, an MTDL with well-balanced affinities for multiple targets can offer additional advantages. So, development of MTDLs for AD is considered as the most promising drug discovery approach.

Carbazole is reported to be a structural component of many natural compounds possessing many valuable medicinal properties which could be helpful in AD treatment. Carbazole derivatives have been reported to possess ChEs inhibitory (Fang et al., 2016), Aβ aggregation inhibitory (Yang et al., 2012), ROS scavenging activities and the ability to protect neurons against oxidative damage (Naik et al., 2010). Numerous carbazole-based hybrid molecules including carbazole-stilbene hybrids (**1**) (Patel, Patel, Kanhed, Teli, Patel, Joshi, et al., 2020), carbazole-aminoadmantane hybrids (**2**) (Makhaeva et al., 2018), sulfonamide derivatives of carbazole (**3**) (Bertini et al., 2017), carbazole-tacrine hybrids (**4**) (Thiratmatrakul et al., 2014) and carbazole-quinoline derivatives (**5**) (Choubdar et al., 2019) (Figure 1(A)) have been reported as potential therapeutic agents for treatment of AD. A wide range of pharmacological activities exhibited by the carbazole derivatives makes carbazole a privileged scaffold in the discovery of new anti-AD agents.

Thiosemicarbazides and acyl hydrazides have received great attention among medicinal chemists as important chemical functionalities due to their wide spectrum of biological activity. Various substituted thiosemicarbazide and acyl hydrazide derivatives have been identified to possess interesting biological activities (Gomes et al., 2014; Mathew et al., 2018; Önkol et al., 2013; Prathima et al., 2012; Sens et al., 2018) (Figure 1(B)). Thiosemicarbazone group is reported to be an indispensable pharmacophore due to its antioxidant and metal chelating properties.

The interesting biological activities associated with the carbazole scaffold, and thiosemicarbazone and acyl hydrazide moieties motivated us to merge these biologically active pharmacophoric groups into a single entity to obtain molecules with multiple beneficial effects for the treatment of AD (Figure 2). Herein, we report the synthesis of carbazole-based thiosemicarbazone and acyl hydrazone derivatives and their biological assessment for possible anti-AD activities.

3. Results and discussion

3.1. Chemistry

The designed carbazole-based thiosemicarbazone and acyl hydrazone derivatives were divided into a set of two series. In series-I, the carbazole scaffold was linked to the substituted thiosemicarbazide moiety (compounds **54–65**) and semicarbazide moiety (compound **66**), while in series-II, it was linked to the acyl hydrazide moiety (compounds **67–73**). Syntheses of these designed compounds are depicted in Schemes 1–3.

The required semicarbazide and thiosemicarbazide intermediates were synthesized as shown in Scheme 1. Substituted benzylamines (**11–15**) were reacted with carbon disulfide and methyl iodide in the presence of triethylamine to obtain methyl carbamodithioate intermediates, which were reacted further with hydrazine hydrate by using methanol as the solvent to give the desired thiosemicarbazide intermediates (**31–35**) (He et al., 2019; Pervez et al., 2017). Similarly, substituted anilines (**16–22**) were reacted with carbon disulfide in the presence of *N,N*-dimethylformamide (DMF) and sodium hydroxide, followed by reaction with hydrazine hydrate to offer the desired thisemicarbazides (**36–42**). The semicarbazide intermediate (**43**) was synthesized from 4-chloroaniline (**23**) in two-step procedure including acylation reaction followed by hydrazinolysis. 4-Chloroaniline (**23**) was acylated by phenyl chloroformate in the presence of sodium carbonate in acetone, followed by reaction with hydrazine hydrate to offer the desired semicarbazide intermediate (**43**).

The required acyl hydrazide intermediates (**44–50**) were synthesized as depicted in Scheme 2. Substituted carboxylic acids (**24–30**) were converted to their respective methyl esters by the Fischer esterification method, and then these esters were converted to the corresponding acyl hydrazides (**44–50**) by refluxing them in methanol with excess hydrazine hydrate.

The designed carbazole-based thiosemicarbazone, semicarbazone and acyl hydrazone derivatives (**52–66**) were synthesized as depicted in Scheme 3. Ethylation of carbazole (**51**) was carried out in the presence of aqueous NaOH solution by using ethyl bromide to obtain *N*-ethylcarbazole (**52**) in high yield. Vilsmeier–Haack formylation reaction of compound (**52**) using DMF, and phosphoryl chloride afforded

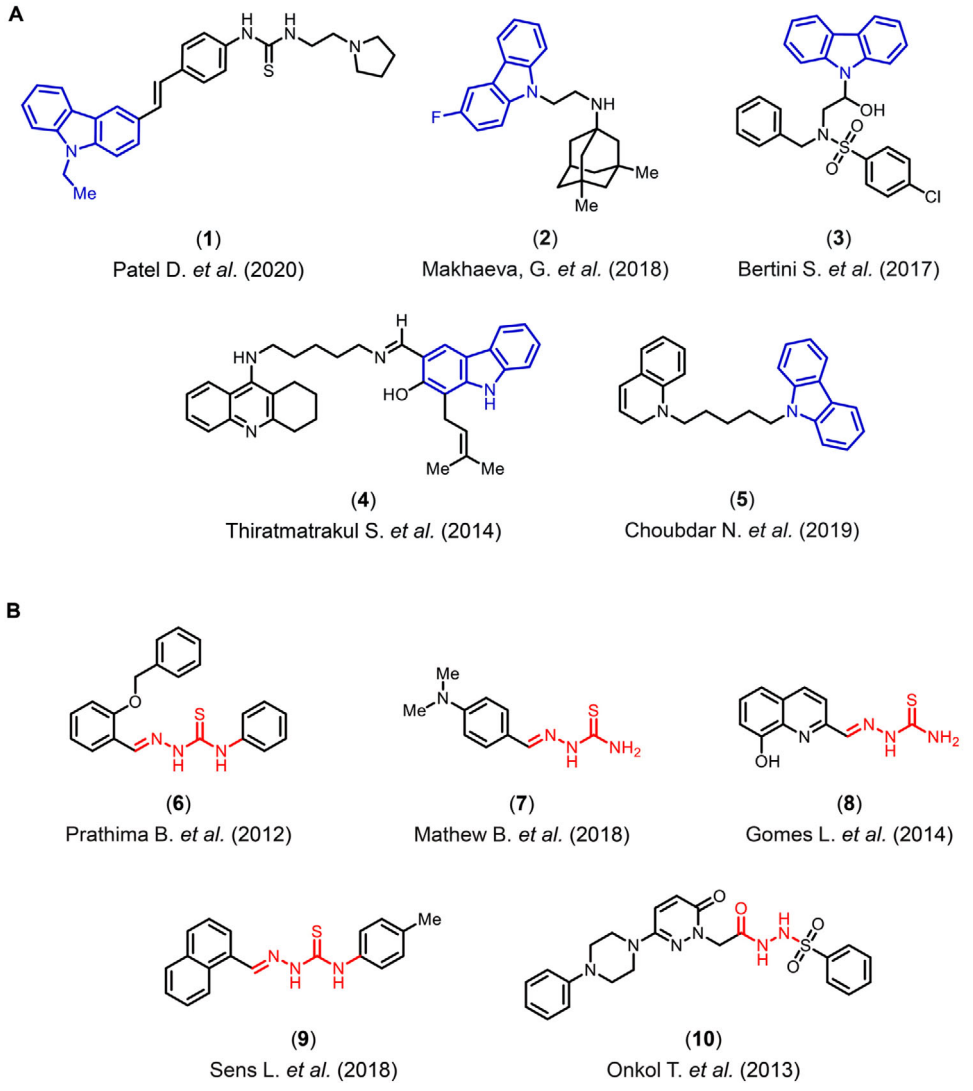

Figure 1. Some reported biologically active (A) carbazole-based compounds (**1**–**5**) and (B) thiosemicarbazone and hydrazide-based compounds (**6**–**10**).

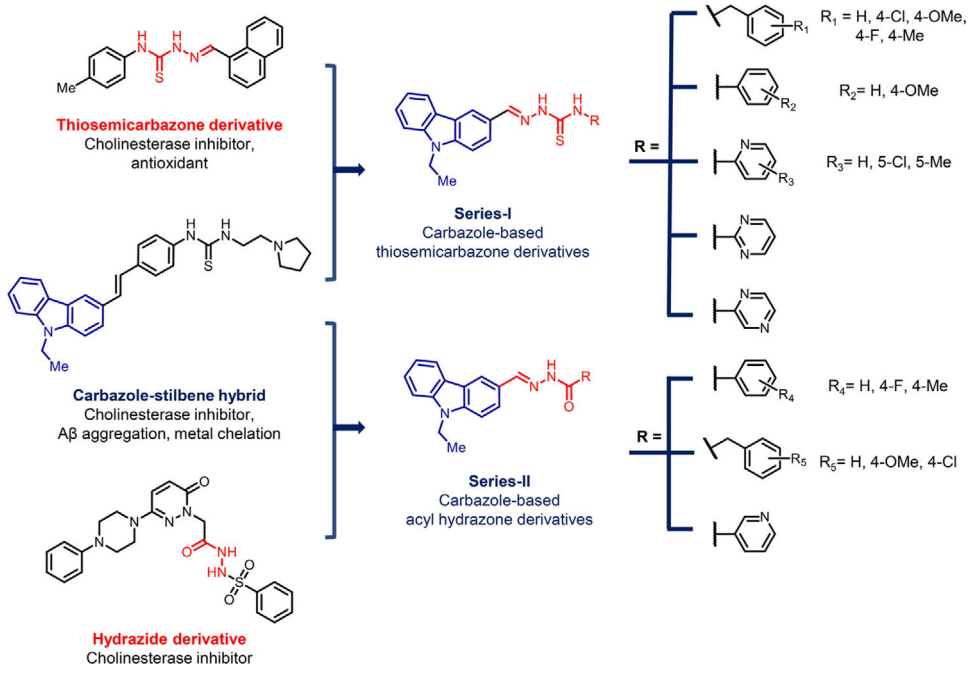

Figure 2. Design aspects of carbazole-based thiosemicarbazone and acyl hydrazone derivatives.

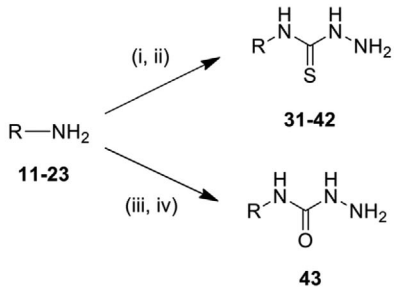

Compd	R =
11, 31	R_1 = H
12, 32	R_1 = 4-OMe
13, 33	R_1 = 4-Cl
14, 34	R_1 = 4-F
15, 35	R_1 = 4-Me

Compd	R =
16, 36	R_1 = H
17, 37	R_1 = 4-OMe
23, 43	R_1 = 4-Cl

Compd	R =
18, 38	R_1 = H
19, 39	R_1 = 5-Cl
20, 40	R_1 = 5-Me

Compd	R
21, 41	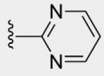
22, 42	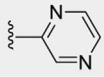

Scheme 1. Synthetic route for the intermediates (**31**–**43**). Reagents and conditions: For compounds (**31**–**35**) (i) carbon disulfide, triethylamine, methanol, 20–30 °C, 2–3 h, methyl iodide in methanol at −10 °C; (ii) hydrazine hydrate, methanol, reflux, 2–4 h. For compounds (**36**–**42**) (i) carbon disulfide, sodium hydroxide, dimethylformamide, 20–30 °C, 2–3 h; (ii) hydrazine hydrate, 70 °C, 1–2 h. For compound (**43**) (i) acetone, potassium carbonate, phenyl chloroformate, sodium bicarbonate, 20–30 °C, 3 h; (ii) hydrazine hydrate, dioxane, reflux, 4 h.

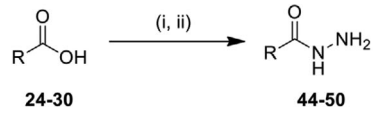

Compd	R =
24, 44	R_1 = H
25, 45	R_1 = 4-OMe
26, 46	R_1 = 4-Cl

Compd	R =
27, 47	R_1 = H
28, 48	R_1 = 4-F
29, 49	R_1 = 4-Me

Compd	R
30, 50	

Scheme 2. Synthetic route for hydrazide intermediates (**44**–**50**). Reagents and conditions: (i) conc. sulfuric acid, methanol, reflux, 6 h; (ii) hydrazine hydrate, methanol, reflux, 2–4 h.

mono-formylated intermediate 9-ethyl-3-formylcarbazole (**53**). Compound (**53**) was condensed with thiosemicarbazide intermediates (**31**–**42**) and semicarbazide intermediate (**43**) in the presence of acetic acid and methanol to yield the thiosemicarbazone derivatives (**54**–**72**) and semicarbazone derivative (**73**), respectively. Similarly, carbazole-based acyl hydrazone derivatives were obtained by condensation of the aldehyde (**53**) with hydrazide intermediates (**44**–**50**) by refluxing in methanol in the presence of catalytic amounts of acetic acid.

3.2. Biological evaluation

3.2.1. In vitro ChE inhibition studies

The *in vitro* ChEs inhibitory activity of the synthesized compounds was determined by Ellman's assay, and protocol of the study was same as described in our previous reports (Kanhed et al., 2015, Kanhed, Patel, Patel, et al., 2020; Sinha et al., 2015). Donepezil and tacrine were taken as the standards for Ellman's assay. The calculated IC_{50} values and selectivity indices of the test compounds for ChEs are reported in Tables 1 and 2. In series-I, thiosemicarbazones (**54**–**65**) showed good ChEs inhibitory activity in micromolar ranges. The benzyl derivative (**54**) exhibited balanced inhibitory activity on both the ChEs (IC_{50} values of 2.21 and 2.33 μM for *h*AChE and *Eq*BuChE, respectively). Introduction of small lipophilic electron-withdrawing fluoro group (in compound **57**) and electron-donating methyl group (in compound **58**) led to a moderate increment in *h*AChE (1.64- and 1.38-fold, respectively) and *Eq*BuChE (1.31-fold for compound **58**) inhibitory activities, whereas introduction of methoxy group (compound **55**) and chloro group (compound **56**) at the *para* position of the benzyl ring resulted into a modest reduction in the inhibitory activities. Replacement of the benzyl ring with phenyl ring (compound **59**) led to a 2.27-fold improvement in the inhibitory activity of *h*AChE (IC_{50} value of 0.97 μM) and a 1.20-fold increase in the inhibitory activity of *Eq*BuChE (IC_{50} value of 1.93 μM). Substitution of the phenyl ring with a methoxyl group at its *para* position (compound **60**) or replacing the phenyl ring with other heterocyclic rings i.e. pyridine (compound **61**), substituted pyridines (compounds **62** and **63**), pyrimidine (compound **64**) or pyrazine (compound **65**) had a detrimental effect, leading to moderate decrease in ChEs inhibitory activities. Substituting the thiosemicarbazone linker with semicarbazone (compound

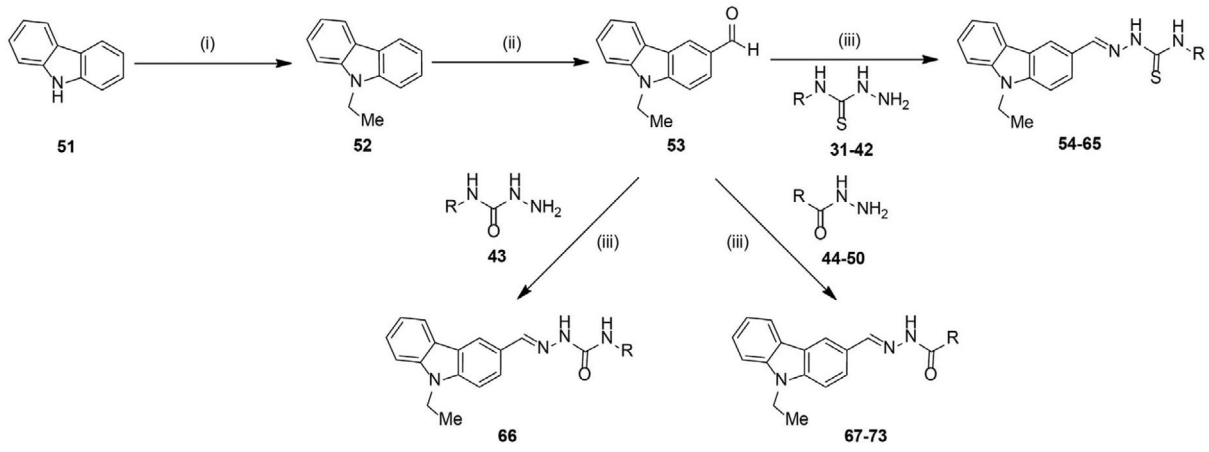

Compd	R =	Compd	R =	Compd	R =	Compd	R
54, 67	R_1 = H	59, 70	R_1 = H	61, 73	R_1 = H	64	
55, 68	R_1 = 4-OMe	60	R_1 = 4-OMe	62	R_1 = 5-Cl	65	
56, 69	R_1 = 4-Cl	66	R_1 = 4-Cl	63	R_1 = 5-Me		
57	R_1 = 4-F	71	R_1 = 4-F				
58	R_1 = 4-Me	72	R_1 = 4-Me				

Scheme 3. Synthetic route for the designed compounds (**54**–**73**). Reagents and conditions: (i) Ethyl iodide, sodium hydroxide, dimethyl sulfoxide, RT, 4–5 h; (ii) phosphoryl chloride, DMF, chloroform, reflux, approx. 12 h; (iii) acetic acid, methanol, reflux, 4–5 h.

66) offered good *h*AChE and moderate *Eq*BuChE inhibitory activities (IC_{50} value of 1.64 μM and 5.57 μM, respectively).

In series-II, acyl hydrazone derivatives (**67–73**) demonstrated good *h*AChE inhibitory and moderate *Eq*BuChE inhibitory activities in micromolar ranges (Table 2). The phenylacetic acid hydrazone derivative (**67**) showed good ChEs inhibitory activity (IC_{50} values of 1.0 μM for *h*AChE and 2.07 μM for *Eq*BuChE). Introduction of a 4-methoxyl group (compound **68**) or 4-chloro group (compound **69**) on the phenyl ring led to a drastic decrease in *Eq*BuChE inhibitory activity. Replacement of the phenylacetic hydrazide moiety with benzhydrazide moiety (compound **70**) did not affect the ChEs inhibitory activities. Incorporation of substituted benzhydrazide moiety (compounds **71** and **72**) and picolinoyl hydrazide moiety (compound **73**) had a detrimental effect, leading to a decrease in ChEs inhibitory activity.

3.2.2. DPPH radical scavenging activity

The DPPH (1,1-diphenyl-2-picrylhydrazyl) radical scavenging assay was used to evaluate the antioxidant activity of the synthesized compounds (Kedare & Singh, 2011). It was determined by the ability of the selected compounds to quench the purple-colored DPPH· radical to a yellow colored stable DPPHH molecule and the corresponding free radical-scavenging potential of the test compounds was calculated by the decline in absorbance of the test solutions at 517 nm. The free radical scavenging activity was calculated as a reduction percentage (RP) of DPPH. Among the tested compounds, compounds (**61** and **62**) exhibited excellent free radical scavenging activity with IC_{50} values of 9.91 and 10.52 μM, respectively, that were near to that of ascorbic acid used as a reference compound (IC_{50} value of 9.01 μM). Donepezil and tacrine were observed to be devoid of any notable radical scavenging activity with IC_{50} values greater than 500 μM (Table 1).

3.2.3. Metal chelation study

Dyshomeostasis of redox transition metals, particularly copper, iron and zinc, and their excessive deposition in the brain have been correlated with AD etiology (Savelieff et al., 2013). Thus, the use of metal ion chelators has been proposed as a possible therapy for a disease like AD. The potential of the test compounds to form chelates with biometals was determined by means of UV–vis spectroscopy (Wang et al., 2015).

Compounds (**61** and **62**) exhibited maximum absorption peaks at 342 and 359 nm respectively, in methanol (as shown in Figure 3). When Cu^{2+} ion solution was added to the solution of the test compounds, a sharp decrease in the heights of the absorbance peaks were observed, indicative of the interactions between the metal ions and the test compounds to form ligand–Cu^{+2} complexes. Insignificant changes in the position and height of absorption peaks were observed when $AlCl_3$, $CaCl_2$, $FeCl_3$ or $FeSO_4$ were added into the test compounds' solutions. This suggests that the test compounds had poor chelating abilities for these ions (Al^{+3}, Ca^{2+}, Fe^{2+} and Fe^{3+}). The test compounds were also evaluated for their binding potential to other key biometal ions, such as Zn^{2+} and Mg^{2+} where these compounds (**61** and **62**) showed negligible binding affinities for these metals. 8-Hydroxyquinoline (8-HQ) was used as a reference compound

Table 1. *In vitro* inhibitory activity on *h*AChE and *Eq*BuChE, and DPPH radical scavenging activities of compounds (**54**–**66**).

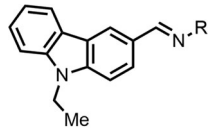

(**54-66**)

Compd	R	IC50 ± SEM (μM) hAChE[a]	IC50 ± SEM (μM) EqBuChE[b]	SI[c]	RP of DPPHd % Inhibition at 100 μM (IC50 ± SEM (μM))
54	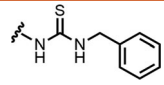	2.21 ± 0.78	2.33 ± 0.65	1.05	24.29 ± 1.93 (>100)
55	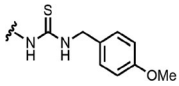	2.20 ± 0.61	4.68 ± 1.03	2.12	20.6 ± 1.37 (>100)
56	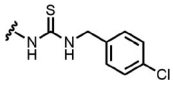	2.63 ± 0.20	4.47 ± 0.42	1.69	21.54 ± 1.23 (>100)
57	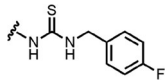	1.35 ± 0.87	2.19 ± 0.98	1.62	26.65 ± 1.11 (>100)
58	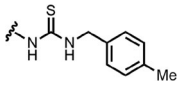	1.60 ± 0.31	1.78 ± 0.19	1.11	25.61 ± 1.98 (>100)
59	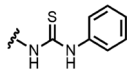	0.97 ± 0.59	1.93 ± 0.68	1.99	83.44 ± 1.66 (35.29 ± 1.43)
60	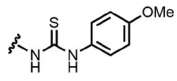	1.59 ± 0.69	1.64 ± 1.09	1.03	10.57 ± 1.29 (>100)
61	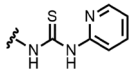	1.37 ± 0.39	2.69 ± 0.40	1.95	85.67 ± 2.09 (9.91 ± 1.12)
62	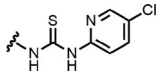	1.18 ± 1.19	3.31 ± 1.12	2.79	84.49 ± 1.87 (10.52 ± 1.43)
63	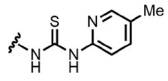	1.30 ± 0.49	4.09 ± 0.44	3.13	83.76 ± 1.51 (40.92 ± 1.39)
64	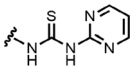	1.98 ± 0.64	5.79 ± 1.17	2.91	nd
65	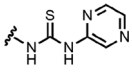	1.43 ± 0.88	2.88 ± 0.98	2.00	nd
66	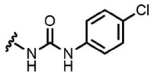	1.64 ± 0.42	5.57 ± 0.91	3.39	15.66 ± 0.93 (>100)
Donepezil		0.04 ± 0.01	1.87 ± 0.08	81.3	5.4 ± 1.11 (>500)
Tacrine		0.05 ± 0.01	0.007 ± 0.00	0.14	17.2 ± 1.19 (>500)
Ascorbic acid		nd	nd	nd	98.26 ± 1.88 (9.01 ± 1.33)

IC_{50}, half maximal inhibitory concentration (mean ± SEM of 3 experiments).
[a]AChE from human erythrocytes.
[b]BuChE from equine serum.
[c]Selectivity Index = IC_{50} (BuChE)/IC_{50} (AChE).
[d]RP of DPPH (%) = Reduction percentage of DPPH at 100 μM.

Table 2. *In vitro* inhibitory activity on *h*AChE and *Eq*BuChE, and DPPH radical scavenging activities of compounds (**67**–**73**).

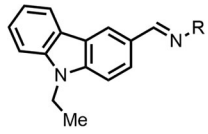

(**67-73**)

Compd	R	IC50 ± SEM (μM) *h*AChE[a]	IC50 ± SEM (μM) *Eq*BuChE[b]	SI[c]	RP of DPPHd % inhibition at 100 μM (IC50 ± SEM (μM))
67	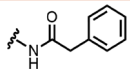	1.00 ± 0.43	2.04 ± 0.69	2.03	14.01 ± 1.33 (>100)
68	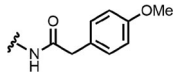	1.11 ± 0.59	3.59 ± 0.83	3.22	7.1 ± 1.13 (>100)
69	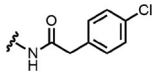	2.04 ± 0.61	23.52 ± 1.33	11.52	10.88 ± 1.25 (>100)
70	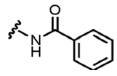	1.10 ± 0.33	2.11 ± 0.81	1.91	10.72 ± 1.13 (>100)
71	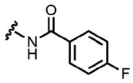	1.94 ± 0.71	4.36 ± 0.71	2.24	10.80 ± 1.39 (>100)
72	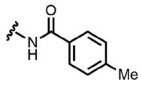	1.64 ± 0.51	5.51 ± 1.23	3.35	1.23 ± 1.09 (>100)
73	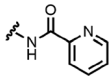	1.88 ± 0.47	19.52 ± 1.28	10.34	nd

IC_{50}, half maximal inhibitory concentration (mean ± SEM of 3 experiments).
[a]AChE from human erythrocytes.
[b]BuChE from equine serum.
[c]Selectivity Index = IC_{50} (BuChE)/IC_{50} (AChE).
[d]RP of DPPH (%) = Reduction percentage of DPPH at 100 μM.

for validation of the assay protocol. A significant alteration in the height and position of absorption peaks was observed when the solutions of the metal ions and the HQ solution were mixed indicating the ability of HQ to form metal–HQ chelates non-selectively.

The above finding asserted the selective Cu^{2+} ion chelation potential of the test compounds (**61** and **62**). Selectivity of these compounds for the copper ions is a crucial factor in the designing of biometal chelating agents to escape binding with other important biometal ions, the imbalance of which could drive to undesired adverse effects.

3.3. Computational studies

3.3.1. Docking studies of compounds (61 and 62) with ChEs

To gain insight into the interactions of the reference compounds and test compounds within the active sites of ChEs, docking studies were performed using Schrodinger Suite (Glide version 5.5 (2009) Schrödinger, LLC, New York, NY). The 3D-crystal structures of *Tc*AChE (PDB code: 2CKM) and *h*BuChE (PDB code: 4BDS) retrieved from RCSB Protein Data Bank (www.rcsb.org/pdb/home/home.do.) were used for this study. Tacrine formed a firm complex with the AChE by making hydrogen bond between the protonated nitrogen of acridine ring of tacrine and C = O of His440 (*h*AChE His447). The aromatic ring of tacrine was observed to be sandwiched between Trp84 and Phe330 (*h*AChE Trp86 and Tyr337). In donepezil, the 1-benzyl moiety of donepezil was observed to be stabilized in the active site by Trp84 and Phe330 residues (*h*AChE Trp86 and Tyr337). The dihydroinden-1-one group of donepezil was stabilized by Trp279 (*h*AChE Trp286) residue through hydrophobic interactions. The 6-methoxy group exhibited H-bonding interaction with Trp279 (*h*AChE Trp286). Tacrine and donepezil, used as standards in biological testing, were also considered for docking with BuChE. The aromatic ring of tacrine stabilized the ligand–receptor complex by π–π interactions with Trp82 of BuChE. H-bonding between amino N-H of tacrine and C = O of His438 imparted further stability to the complex. While in case of donepezil, the benzyl group was found to be stabilized by Trp82. The dihydroinden-1-one group stabilized the ligand–receptor complex by means of hydrophobic interactions with Ser198, Trp231 and Phe398. The interaction view of **61** within the active site of AChE is represented in Figure 4(A,B) (Patel, Patel, Kanhed, Teli, Patel, Gandhi, et al., 2020). The active site

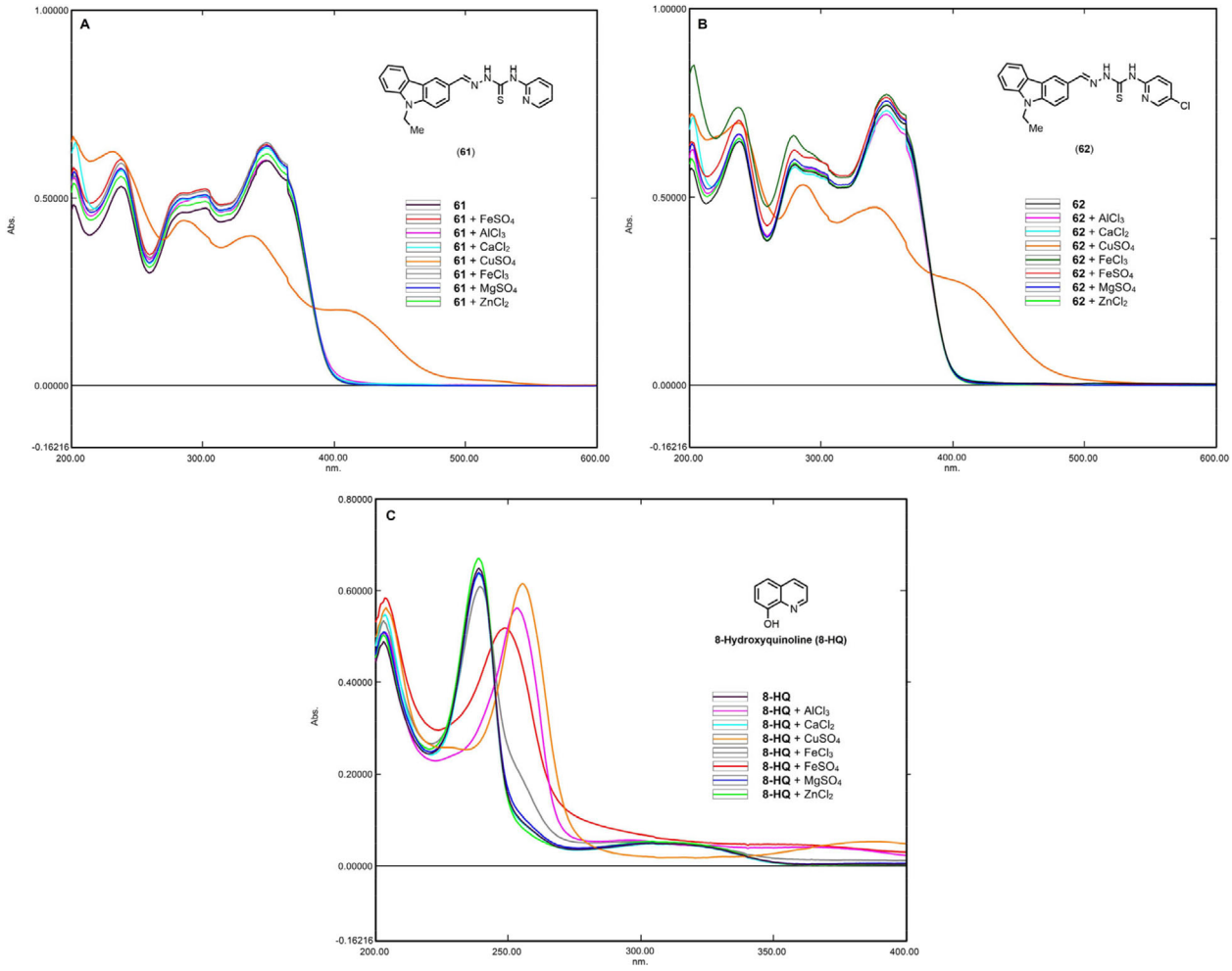

Figure 3. Biometal chelation study of compounds (**61**, **62**) and HQ. The UV–vis absorption spectra of (A) compound (**61**), (B) compound (**62**) and (C) 8-HQ at 25 μM concentration alone and in presence of $AlCl_3$ (25 μM), $CaCl_2$ (25 μM), $CuSO_4$ (25 μM), $FeCl_3$ (25 μM), $FeSO_4$ (25 μM), $MgSO_4$ (25 μM) and $ZnCl_2$ (25 μM) in methanol at room temperature.

of AChE consists of an oxyanion hole, an acyl-binding pocket, catalytic active site (CAS) and peripheral anionic site (PAS). The key amino acid residues responsible for binding are Trp84 and Phe330 in the CAS, and Trp279 in the PAS. The docking study shows that compound (**61**) is fitting intimately inside the groove formed by Trp84, Tyr121 and Phe330 amino acid residues. It was positioned along the active site gorge similar to donepezil, starting from the active site amino acid residue Trp84 to the peripheral site amino acid residue Trp279. The pyridine ring of compound (**61**) was sandwiched between Trp84 and Phe330 residues of CAS. It showed π–π stacking interactions with Trp84 (3.9 Å) and Phe330 (3.6 Å). The tricyclic carbazole ring was positioned near the Trp279 residue of CAS. Binding mode of the compound (**61**) within the active site of BuChE is depicted in Figure 4(C,D). Precise analysis of interaction of **61** in the active site of BuChE showed that the key hydrogen bonding interaction observed experimentally for the tacrine moiety with His438 residue was maintained for compound (**61**). In addition, nitrogen atom of the pyridine ring formed a hydrogen bond with Trp-82 (2.8 Å). The -NH of semicarbazone group showed hydrogen bonding with His438 (2.0 Å). The tricyclic carbazole ring showed T-shape edge-to-edge π–π stacking interactions with Trp231 (4.8 and 4.9 Å). In the structure of BuChE, Trp82 amino acid residue is conserved, but Phe330 present in AChE is replaced by Ala328 in BuChE. Absence of phenylalanine residue influences the affinity of compounds for BuChE.

Similarly, the interaction views of **62** within the active sites of AChE and BuChE are represented in Figure 5. Compound (**62**) fits compactly inside the groove formed by amino acid residues Trp84, Try121 and Phe330. 5-Chloropyridine ring of compound (**62**) was oriented near Trp84 and Phe330 residues of CAS. The tricyclic carbazole ring was positioned near Trp279 residue of CAS. In case of BuChE, the tricyclic carbazole ring of compound (**62**) showed T-shaped edge-to-edge π–π stacking interactions with Trp231 (4.8 and 4.9 Å) and Phe329 (5.3 and 5.5 Å). 5-Chloropyridine ring was oriented parallel to Trp82 residue in CAS. The -NH of semicarbazone group was observed to form a hydrogen bond with His438 (2.4 Å).

3.3.2. Molecular dynamics simulation studies

To determine the conformational stability and promising molecular interactions of compounds (**61**) and (**62**) in the active sites of ChEs, time-dependent molecular dynamics (MD) stability analysis was performed. The MD simulations

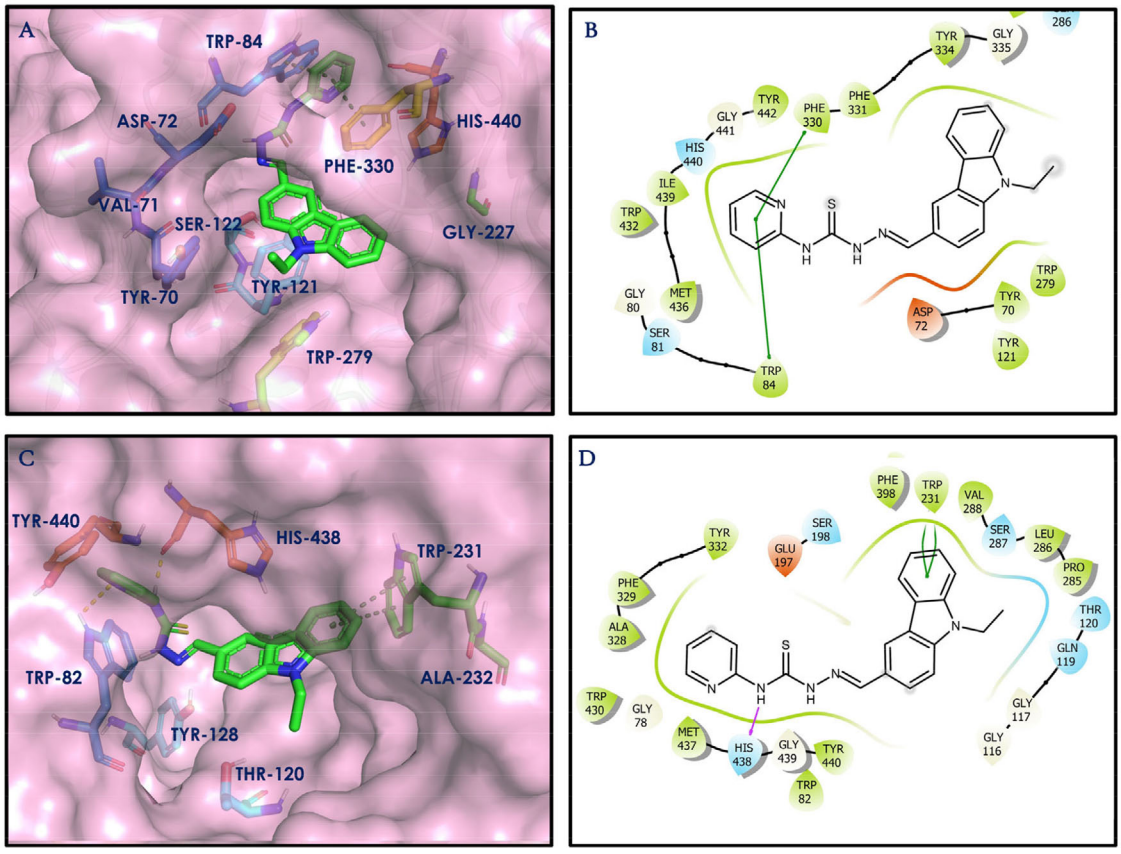

Figure 4. Docking poses of compound (**61**) with *Tc*AChE (PDB ID: 2CKM) and *h*BuChE (PDB ID: 4BDS). (A, C) Binding modes of **61** within the active sites of *Tc*AChE and *h*BuChE, respectively. Ligand is shown as green sticks. Hydrogen bonds and π–π interactions are shown as yellow and green dashed lines, respectively. (B, D) 2D-ligand interaction diagrams of **61** with *Tc*AChE and *h*BuChE, respectively.

were performed for a period of 50 ns using GROMACS2020.1. The study was performed using the docked pose of the ligand–receptor complex as the reference frame. The conformational changes and dynamic behavior in complexes were analyzed by various computational parameters like root-mean-square deviation (RMSD)-P, RMSD-L, root-mean-square fluctuation (RMSF)-P (P = protein, L = ligand) and solvent accessible surface area (SASA) for protein while having ligand in the receptor active site are shown in Figures 6–9.

The protein RMSD is determined mainly to understand the extent of movement of receptor atoms or groups while having the ligand inside the receptor active site. This type of analysis is indicative of the stability of conformation of the receptor structure and deviation over a period of time. The average RMSD-P for AChE in complexation with the docked compound (**61**) was 0.1386 nm (range of 0.08–0.253) (Figure 6(A)). This suggests that over a period of time the protein having compound (**61**) in the active site was quite stable. The average RMSD-L was 0.3497 nm (range of 0.2–0.48 nm) which strongly indicated the stability of the protein–ligand complex without a major deviation in orientation of the compound in the receptor active site over the period of MD analysis (Figure 6(B)). RMSF indicates the integrity of the structure and mobility of the residues in the protein structure. It shows the flexibility of each amino acid residue of the protein upon binding to the ligand. Here, all the residues of the protein structure including loop and terminal residues, with compound (**61**) docked in the receptor active site, showed RMSF-P within 0.35 nm (Figure 6(C)). Apart from these observations, SASA analysis also supported the stability of the protein–ligand complex (Figure 6(D)). The short-range electrostatic (Coul-SR) and van der Waals/hydrophobic (LJ-SR) interaction energies of the protein–ligand complex suggested potential electrostatic and hydrophobic interactions. The average values of Coul-SR and LJ-SR were observed to be −57.14 ± 1.90 kJ/mol and −182.43 ± 2.10 kJ/mol respectively, suggesting that the contribution of hydrophobic interactions was higher than the electrostatic interactions in stabilizing the protein–ligand complex.

In a similar way, the MD analysis of compound (**61**) docked in the BuChE active site was also carried out. The average RMSD-P was 0.156 nm (range of 0.10–0.218 nm) (Figure 7(A)) and the RMSD-L was found in the range of 0.14–0.43 nm (Figure 7(B)). Including terminal and loop residues, the observed RMSF-P for all the residues was below 0.25 nm (Figure 7(C)). SASA analysis also supported the stability of the protein–ligand complex (Figure 7(D)).The short-range electrostatic (Coul-SR energy value of −76.14 ± 2.9 kJ/mol) and van der Waals/hydrophobic (LJ-SR energy value of −172.43 ± 2.7 kJ/mol) interaction energies explained promising electrostatic and hydrophobic interactions between the protein and the ligand. The obtained values suggested that the role of hydrophobic interactions was much more than

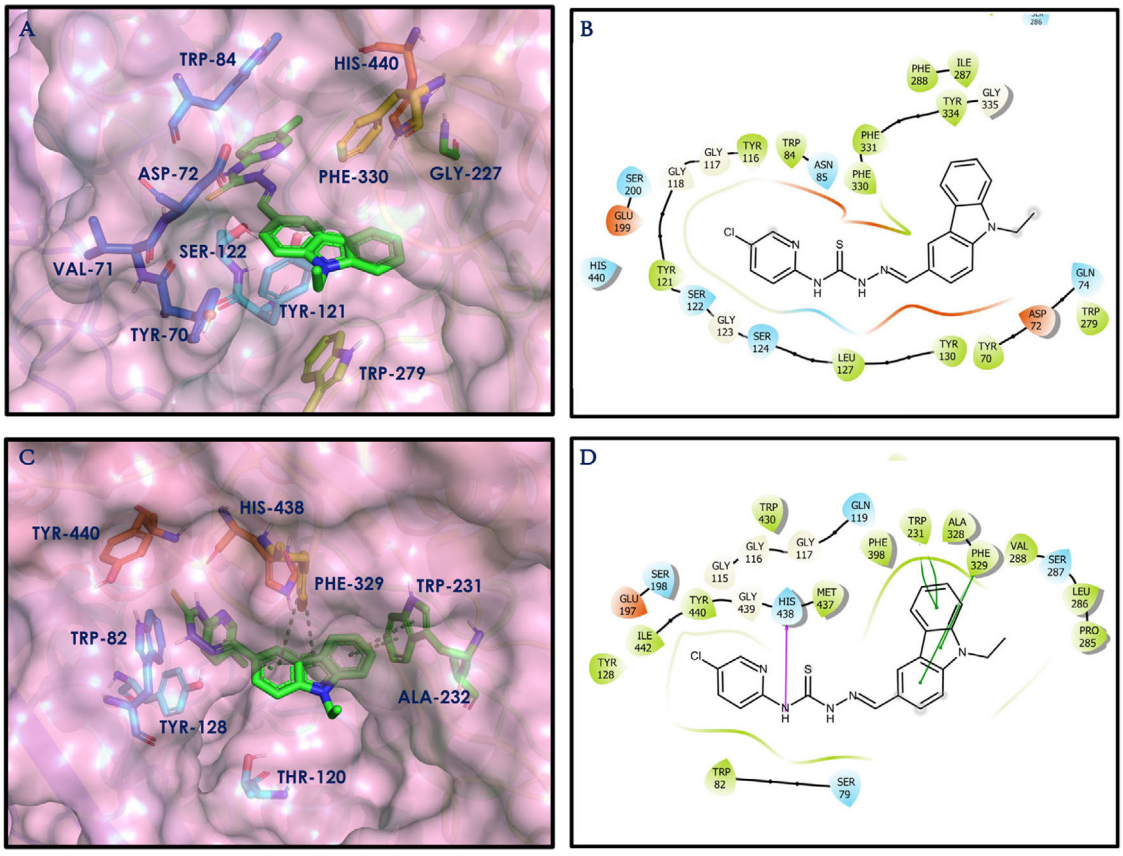

Figure 5. Docking poses of compound (**62**) with *Tc*AChE (PDB ID: 2CKM) and *h*BuChE (PDB ID: 4BDS). (A, C) Binding modes of **62** within the active sites of *Tc*AChE and *h*BuChE, respectively. Ligand is shown as green sticks. Hydrogen bonds and π–π interactions are shown as yellow and green dashed lines, respectively. (B, D) 2D-ligand interaction diagrams of **62** with *Tc*AChE and *h*BuChE, respectively.

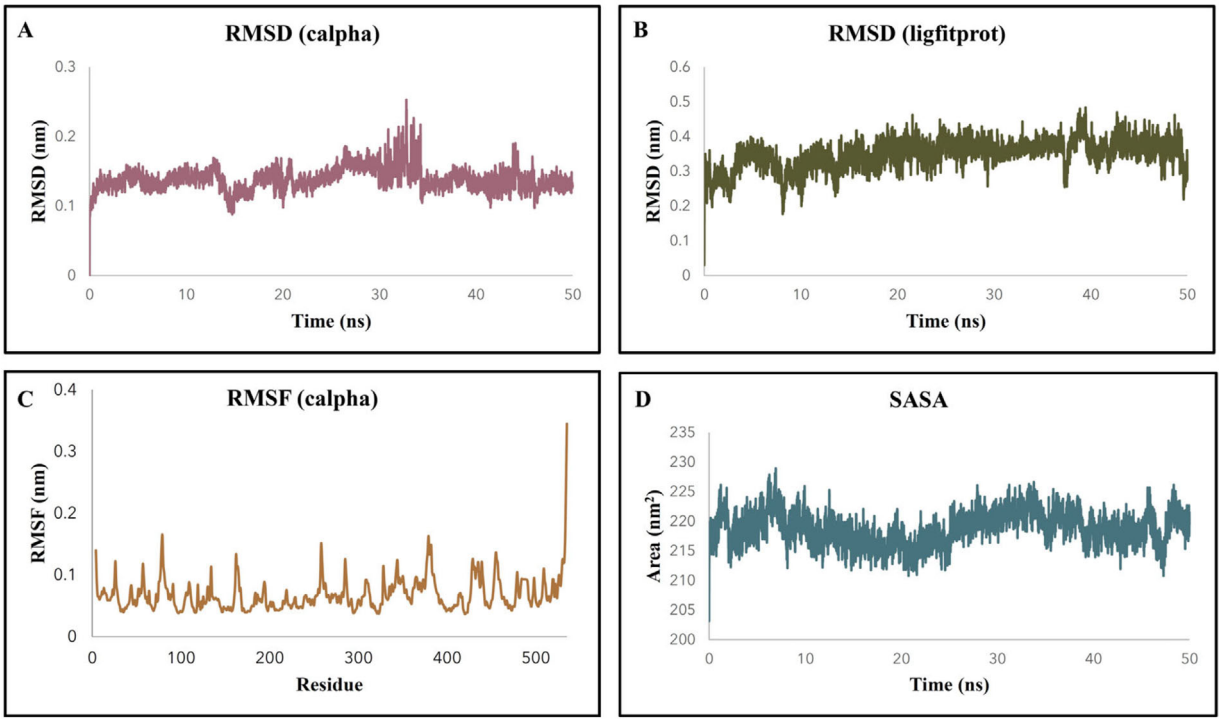

Figure 6. Molecular dynamics simulation of compound (**61**) with AChE as a function of time. (A) RMSD-P, (B) RMSD-L, (C) RMSF-P, and (D) SASA for AChE with compound (**61**).

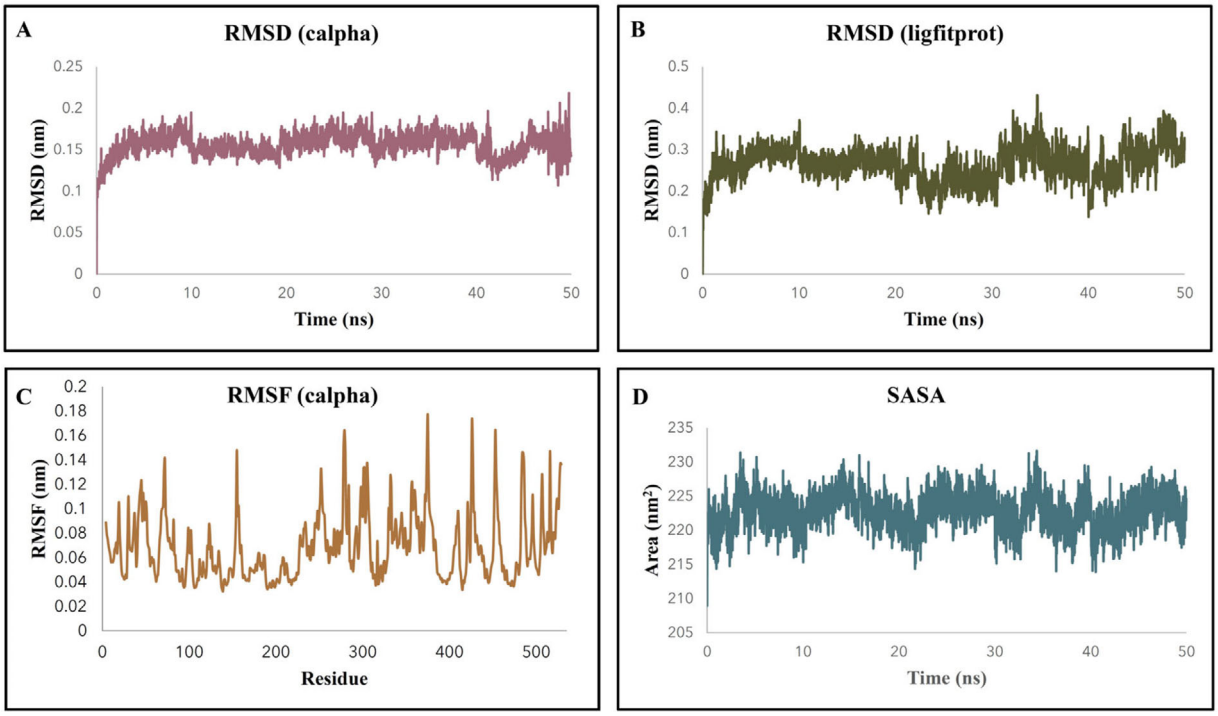

Figure 7. Molecular dynamics simulation of compound (**61**) with BuChE as a function of time. (A) RMSD-P, (B) RMSD-L, (C) RMSF-P and (D) SASA plots for BuChE with compound (**61**).

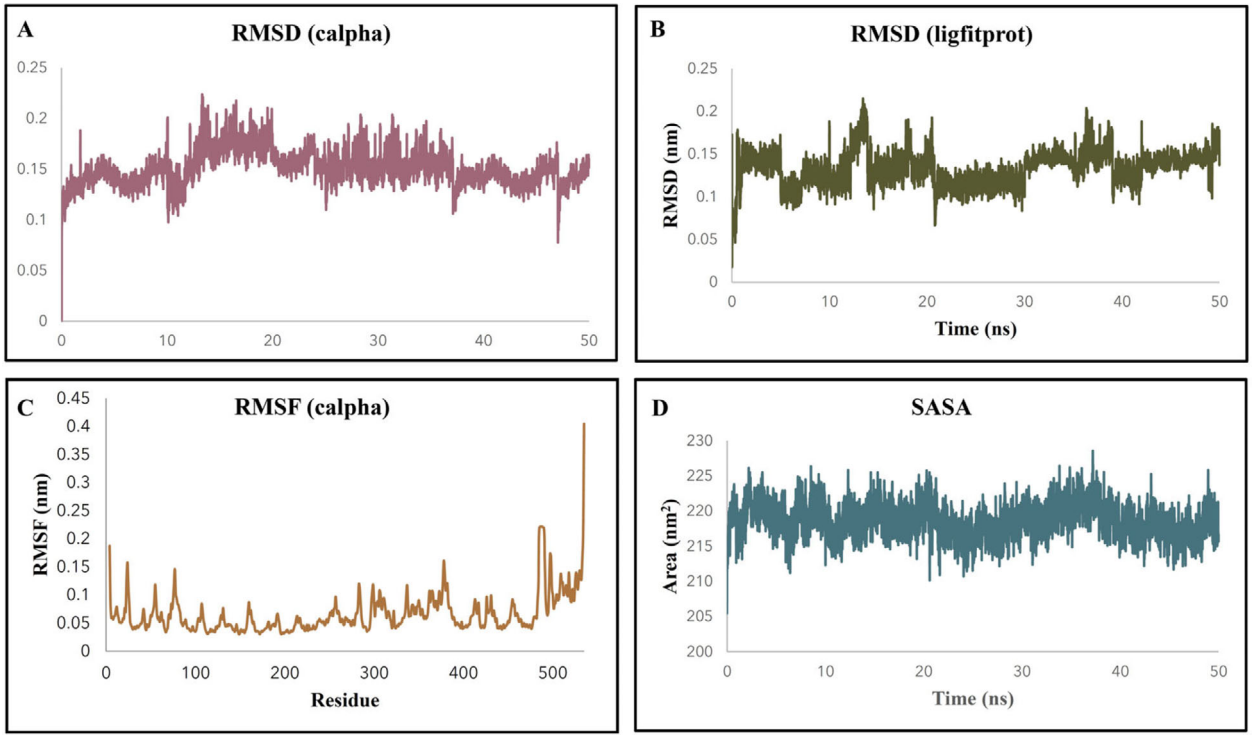

Figure 8. Molecular dynamics simulation of compound (**62**) with AChE as a function of time. (A) RMSD-P, (B) RMSD-L, (C) RMSF-P and (D) SASA plots for AChE with compound (**62**).

the electrostatic interactions in stabilizing the ligand within the protein.

Similar MD simulation studies for ChEs with compound (**62**) were also performed. For compound (**62**) with AChE, the average RMSD-P of 0.151 nm (range of 0.08–0.223 nm) suggested high stability of the receptor with compound (**62**) in the active site (Figure 8(A)). RMSD-L was observed to be 0.134 nm with a range of 0.08–0.214 nm (Figure 8(B)). Here, the observed overall RMSF-P value was below 0.45 nm supporting the stability of the protein while having the ligand in the receptor active cavity (Figure 8(C)). Apart from these observations, SASA analysis also supported the stability of

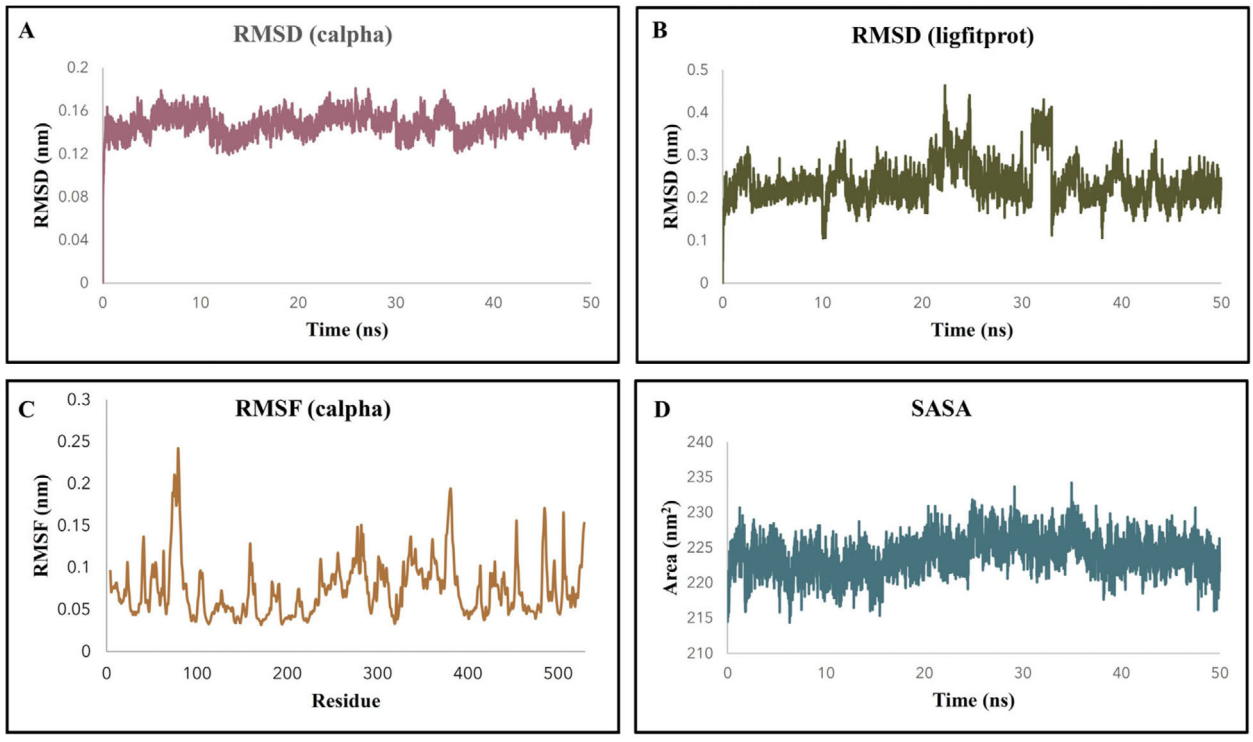

Figure 9. Molecular dynamics simulation of compound (**62**) with BuChE as a function of time. (A) RMSD-P, (B) RMSD-L, (C) RMSF-P and (D) SASA plots for BuChE with compound (**62**).

the protein–ligand complex (Figure 8(D)). Here again, the short-range electrostatic (Coul-SR energy value of –61.34 ± 1.6 kJ/mol) and van der Waals/hydrophobic (LJ-SR energy of –206.73 ± 2.4 kJ/mol) interaction energies explained strong interactions between the protein and the ligand.

The RMSD-P value for BuChE-compound (**62**) complex was 0.148 nm (range 0.12–0.18 nm) explaining high stability of the protein (Figure 9(A)). The average RMSD-L was 0.237 nm (range of 0.1–0.46 nm) (Figure 9(B)) and RMSF-P was less than 0.35 nm including loop and terminal residues (Figure 9(C)). Here also the hydrophobic interaction contribution was found to be higher than the electrostatic interactions (found Coul-SR energy and LJ-SR energy values were –66.14 ± 2 kJ/mol and –192.46 ± 1.8 kJ/mol, respectively).

3.3.3. In silico *prediction of physicochemical and pharmacokinetics parameters*

Determination of pharmacokinetics properties of the lead molecules is an important step in the drug discovery process to prevent the drug attrition in the later stages of clinical trials due to inadequate absorption, distribution, metabolism, excretion, and toxicity (ADMET) profile. Application of computer-based tools in prediction of ADMET indicators is attracting considerable attention to screen out such outliers in the very early stages of the drug discovery process. Here, the ADMET parameters for the most promising compounds (**61** and **62**) along with the standard drugs donepezil and tacrine were assessed using QikProp module of Schrodinger Suite (Table 3), and pkCSM web server (http://structure.bioc.cam.ac.uk/pkcsm) (Table 4).

As shown in Table 3, compounds (**61** and **62**) obeyed all of the Lipinski's rule-of-five parameters in the given permissible ranges. Veber et al. introduced two additional key parameters viz. number of rotatable bonds (NRB) and topological polar surface area (TPSA) (Veber et al., 2002). NRB describes the conformational flexibility of the molecules. For better oral bioavailability and drug-likeness, a molecule should have lesser than 8 rotatable bonds or 7 atoms in a linear chain outside the ring. TPSA is a measure of polarity. It is a major determinant of passive diffusion of a molecule through biological membranes and thus, it enables the prediction of drug absorption, including bioavailability, blood–-brain barrier (BBB) permeation and intestinal absorption. Lenz and coworker have reported an average TPSA value to be less than 90 Å^2 for a central nervous system (CNS) active drug (Pajouhesh & Lenz, 2005). The average value for marketed CNS drugs is 40.5 Å^2 (range 4.63–108 Å^2). Both the compounds (**61** and **62**) have NRB values of six and TPSA values of ~56.5 Å^2. QPCaco-2 value correlates the oral absorption of a drug predicting its gut–blood barrier permeability. Values higher than 500 predict significant oral absorption, which was attained by both the test compounds. Significant quantum of oral bioavailability of the test compounds is further supported by the predicted human oral absorption percent (% HOA) values. The *n*-octanol-water partition coefficient (QPlog$P_{o/w}$), brain/blood partition coefficient (QPlogBB), CNS and apparent MDCK (Madin-Darby canine kidney) cell permeability (QPPMDCK) collectively predict the potential of a ligand to cross the BBB. Compounds (**61** and **62**) are predicted to have borderline CNS penetration as they possess CNS values of zero, and QPlogBB values of –0.276 and –0.113, respectively. QPPMDCK value is a good criterion

Table 3. ADMET indicators of compounds (**61** and **62**), donepezil and tacrine predicted by QikProp.

Parameters	Limits	Compd (61)	Compd (62)	Donepezil	Tacrine
MW	130–725	373.475	407.92	379.498	198.267
HBD	0–6	2	2	0	1.5
HBA	2–20	5	5	5.5	2
NRB	0–8	6	6	6	1
PSA	7–200	56.493	56.502	46.234	33.825
QPlog$P_{o/w}$	–2 to 6.5	5.002	5.496	4.242	2.536
Volume	500–2000	1220.936	1265.381	1248.451	701.299
SASA	300–1000	713.155	737.436	681.675	425.06
ReFG	0–2	0	0	0	0
Rule of five (Violation)	0–1	1	1	0	0
CNS	–	0	0	1	1
QPPMDCK	–	2955.75	7323.718	589.289	1602.036
QPPCaco	–	2565.936	2562.007	1070.771	2965.755
QPlogBB	–3 to 1.2	–0.276	–0.113	0.223	0.047
QPlog*S*	–6.5 to 0.5	–6.753	–7.495	–4.059	–3.036
QPlogK_{hsa}	–1.5 to 1.5	0.673	0.788	0.516	0.049
% HOA	0–100	100	100	100	100
#star	0–5	2	1	0	0

MW, molecular weight; HBD, hydrogen-bond donor atoms; HBA, hydrogen-bond acceptor atoms; NRB, number of rotatable bonds; PSA, polar surface area; QPlog$P_{o/w}$, predicted octanol/water partition coefficient; SASA, total solvent accessible surface area; ReFG, reactive functional groups; QPPMDCK, predicted apparent MDCK cell permeability in nm/s; QPPCaco, caco-2 cell permeability in nm/s; QPlogBB, brain/blood partition coefficient; QPlog*S*, predicted aqueous solubility; QPlogK_{hsa}, binding to human serum albumin; % HOA, human oral absorption on 0-100% scale; #star, number of parameters which fall outside the 95% range of similar values for the known drugs.

Table 4. ADMET descriptors determined by pkCSM tool.

			Predicted values	
Sr. no.	Property	Model name	61	62
1	Absorption	Water solubility (log mol/L)	–4.916	–5.282
2		Caco2 permeability (log Papp in 10^{-6} cm/s)	1.21	1.163
3		Human intestinal absorption (% absorbed)	94.176	92.346
4		Skin permeability (log K_p)	–2.727	–2.723
5		P-glycoprotein substrate	Yes	Yes
6		P-glycoprotein I inhibitor	Yes	Yes
7		P-glycoprotein II inhibitor	Yes	Yes
8	Distribution	Human VDss (log L/kg)	0.606	0.526
9		Human fraction unbound (Fu)	0.056	0.031
10		BBB permeability (log BB)	0.082	0.063
11		CNS permeability (log PS)	–1.783	–1.648
12	Metabolism	CYP2D6 substrate	No	No
13		CYP3A4 substrate	Yes	Yes
14		CYP1A2 inhibitor	Yes	Yes
15		CYP2C19 inhibitor	Yes	Yes
16		CYP2C9 inhibitor	Yes	Yes
17		CYP2D6 inhibitor	No	No
18		CYP3A4 inhibitor	Yes	Yes
19	Excretion	Total clearance (log mL/min/kg)	–0.174	–0.128
20		Renal OCT2 substrate	No	No
21	Toxicity	AMES toxicity	No	Yes
22		Human max. tolerated dose (log mg/kg/day)	–0.195	–0.118
23		hERG I inhibitor	No	No
24		hERG II inhibitor	Yes	Yes
25		Oral rat acute toxicity (LD_{50}, mol/kg)	2.326	2.294
26		Oral rat chronic toxicity (LOAEL) (log mg/kg_bw/day)	0.895	0.97
27		Skin sensitization	No	No
28		Minnow toxicity (log mM)	0.392	0.204

for the prediction of BBB permeation. A QPPMDCK value greater than 500 is considered as good, and the test compounds displayed significantly high values for this parameter. QPlogK_{hsa} predicts the binding of test molecules to the human serum albumin. The test compounds (**61** and **62**) show adherence to the recommended values. The descriptor '#star' annotates the number of parameters having values falling outside the 95% range of the same values for the reported drugs. A larger number of #star suggests that a molecule is less druglike than molecules with lesser #stars. Compounds (**61** and **62**) showed values of #star within the limit, thus they could be taken as drug-like compounds.

pkCSM tool was employed to predict some additional ADMET properties. Some of these descriptors are mentioned in Table 4. Compounds (**61** and **62**) are predicted to have good absorption values suggesting high chances of crossing the gut by passive diffusion. The water solubility, Caco2 permeability, human intestinal absorption and skin permeability values for the test compounds were observed to be in acceptable ranges. The test ligands (**61** and **62**) are predicted

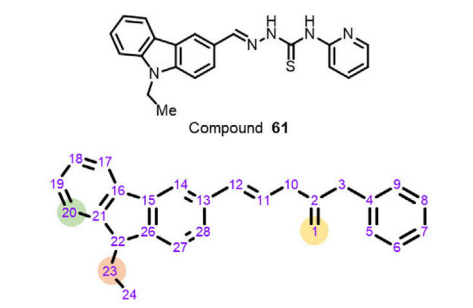

Ranking	Atom	Score	Energy	2DSASA
1	S.1	35.0	43.5	65.0
2	C.23	55.3	63.9	28.7
3	C.20	59.7	68.2	26.6
4	C.26	61.4	68.2	23.8
5	C.19	64.8	74.1	32.7
6	N.3	65.7	72.0	11.7
7	C.17	66.1	74.1	26.1
8	N.10	66.7	72.0	13.2
9	C.27	67.7	74.1	26.1
10	N.9	67.8	75.6	21.4

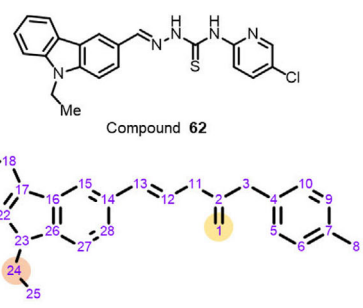

Ranking	Atom	Score	Energy	2DSASA
1	S.1	35.4	43.5	65.0
2	C.24	55.3	63.9	28.7
3	C.21	59.6	68.2	26.6
4	C.27	61.2	68.2	23.8
5	C.20	64.8	74.1	32.7
6	N.3	66.0	72.0	11.7
7	C.18	66.1	74.1	26.1
8	N.11	67.0	72.0	13.2
9	C.28	67.6	74.1	26.1
10	C.15	67.8	74.1	19.5

Figure 10. SOM prediction using SMARTCyp web server for compounds (**61** and **62**). The top three sites of metabolism were highlighted in colored circles at respective positions in their chemical structures. Tables show the list of top 10 metabolic sites of the lead molecules based on their scores and energies.

to have high VDss (volume of distribution at steady-state) (values of 4.036 and 3.357 L/kg, respectively). BBB and CNS permeability values of the test compounds were also acceptable when compared with the standard values. The results indicated that these compounds were likely to cross these barriers. Metabolism of any drug molecule depends mainly on the action of the cytochrome (CYP) class of enzymes. The lead molecules (**61** and **62**) were predicted to be the substrates for CYP3A4 suggesting possible metabolism of these compounds with the action of CYP3A4. They were also predicted to be the inhibitors of CYP1A2, CYP2C19, CYP2C9 and CYP3A4 which could cause interference with the metabolism of other drugs metabolized by these isoforms. The predicted excretion values also supported drug-like behavior of the test compounds based on the total clearance and interaction with renal organic cation transporter 2 (OCT2). The test ligands were found to be non-substrates of OCT2 predicting their proper renal clearance. Compounds (**61** and **62**) were predicted to have maximum tolerated doses (human) of 0.638 and 0.762 mg/kg/day, respectively. The AMES test predicts the non-mutagenic and non-carcinogenic nature of compound (**61**), whereas compound (**62**) was predicted to have possible mutagenic and/or carcinogenic properties. Furthermore, the lead molecules were found to be non-inhibitors of human Ether-a-Go-go Related Gene-I (hERG-I) and hERG-II channels. The minnow toxicity was found to be higher than −0.3 log mM which predicted that the test ligands were acutely nontoxic. All these results together indicate that the lead molecules (**61** and **62**) have drug-like pharmacokinetics profiles, which would increase their biological significance.

3.3.4. Site of metabolism prediction by SMARTCyp

The test compounds (**61** and **62**) were predicted to be metabolized by CYP3A4 isoform. Common sites of metabolism (SOM) of the test ligands were predicted using the SMARTCyp web server (https://smartcyp.sund.ku.dk/mol_to_som). For the validation of SMARTCyp predictions, verapamil, a substrate of CYP3A4 was used as its metabolic products, was well reported. The predicted SOM of verapamil by SMARTCyp was in accordance with the literature (Sun et al., 2004). As predicted by SMARTCyp (Figure 10), the primary SOM in compounds (**61** and **62**) is S.1 of thiocarbonyl group of semicarbazone as it ranked first with the least scores and energies. The secondary predicted SOM are C.20 and C.21 sites on the carbazole ring of compound (**61** and **62**) respectively, while the tertiary predicted SOM are the C.23 and C.24 methylene carbons of ethyl group attached to the carbazole ring of compounds (**61**) and (**62**), respectively.

4. Conclusion

In conclusion, a series of carbazole-based thiosemicarbazone, semicarbazone and hydrazone derivatives were designed, synthesized and biologically evaluated for their ChE inhibitory, antioxidant and biometal chelating properties. *In vitro* study showed that the synthesized compounds possessed ChE inhibitory activity with IC_{50} values ranging between 0.9 and 2.6 μM for *h*AChE and 1.6 and 23.32 μM for *Eq*BuChE. Among them, compounds (**61** and **62**) showed good *h*AChE inhibitory activities (IC_{50} values of 1.37 and 1.18 μM, respectively) while exhibited moderate *Eq*BuChE inhibitory activities (IC_{50} values of 2.69 and 3.31 μM, respectively). These compounds also exhibited excellent antioxidant activity. Compounds (**61** and **62**) showed selective copper metal chelating properties without affecting other biometals.

Molecular dynamics simulation and molecular docking studies indicated close interactions of the most promising compounds in the active sites of ChEs. In addition, compounds (**61** and **62**) were predicted to have *in silico* drug-like ADMET properties. Findings of the present study suggest compounds (**61** and **62**) as promising leads for further development as balanced MTDLs to be used as anti-AD agents.

5. Experimental

General: All the required reagents and solvents for the experiments were procured from commercial suppliers such as Sigma Aldrich and Spectrochem. The solvents and chemicals were purified whenever required by basic laboratory techniques prior to use. The silica gel 60 GF_{254} (Merck) TLC plates having a thickness of 0.25 mm were used to observe the progress of the reaction by visualizing in a UV (254 nm) chamber and/or exposure to various staining reagents. Melting points of the synthesized intermediates and final compounds were recorded in a glass capillary using a VEEGO melting point apparatus having a silicone oil bath and a temperature resolution of 0.1 °C. The IR spectra were obtained using FTIR spectrophotometer [Bruker ALPHA-T (Germany)] using KBr pellets. The ^{1}H NMR spectra were acquired on a Bruker 400 MHz spectrometer in deuterated solvents. The chemical shift (δ) values are expressed in parts per million (ppm) in relation to tetramethylsilane (TMS) as internal standard. The pattern of the peaks is expressed as s (singlet), d (doublet), dd (doublet of doublet), t (triplet), q (quartet) and m (multiplet). The mass spectrometer of Thermo Fisher with electrospray ionization (ESI) ion source was used for the recording of mass spectra.

5.1. Chemistry

5.1.1. General method for the synthesis of 4-substituted thiosemicarbazide intermediates (31–42)

For intermediates (31–35) (Method A): To a stirred solution of substituted benzylamines (**11–15**) (1 equiv.) and triethylamine (1.5 equiv.) in methanol (10 mL), a solution of carbon disulfide (1.2 equiv.) in methanol (5 mL) was added gradually. The resulting mixture was allowed to stir for 2–3 h at room temperature (RT). To it, methyl iodide (1 equiv.) in methanol (5 mL) was slowly added keeping temperature of the reaction mixture at –10 °C. After complete addition, the reaction mixture was stirred for additional 2 h at RT. After completion of the reaction as checked by TLC, the reaction mixture was concentrated under reduced pressure and partitioned between 30 mL of ether and 0.2 N HCl solution. The ethereal layer was washed with cold water and saturated with NaCl solution, dried using anhydrous $MgSO_4$, filtered and evaporated under vacuum to obtain white solid mass. The obtained solid mass was further charged to a solution of hydrazine hydrate (3 equiv.) in methanol (15 mL). The resulting reaction mixture was refluxed for 4 h. After completion of the reaction as confirmed by TLC, the reaction mixture was allowed to attain RT. The solid so precipitated were collected by filtration and washed with cold methanol to obtain the desired intermediates (31–35).

5.1.1.1. N-Benzylhydrazinecarbothioamide (31).

The intermediate (**31**) was synthesized as per the general Method A from benzylamine (**11**) (1.0 g, 9.33 mmol) as white solid (He et al., 2019). (Yield: 60%); m.p. 126–128 °C (lit m.p. 129–130 °C); IR (KBr, cm^{-1}): 3328, 3027, 2917, 1618, 1225, 1085; MS (*m/z*): 182.0 $[M+H]^+$.

5.1.1.2. N-(4-Methoxybenzyl)hydrazinecarbothioamide (32).

The intermediate (**32**) was synthesized as per the general Method A from 4-methoxybenzylamine (**12**) (1.0 g, 7.29 mmol) as white solid (Pervez et al., 2017). (Yield: 62%); m.p. 112–114 °C; IR (KBr, cm^{-1}): 3332, 3036, 2914, 1616, 1248, 1029; MS (*m/z*): 212.0 $[M+H]^+$.

5.1.1.3. N-(4-Chlorobenzyl)hydrazinecarbothioamide (33).

The intermediate (**33**) was synthesized as per the general Method A from 4-chlorobenzylamine (**13**) (1.0 g, 7.06 mmol) as white solid (Pervez et al., 2018). (Yield: 62%); m.p. 178–180 °C; IR (KBr, cm^{-1}): 3317, 2982, 2926, 1615, 1238, 1083, 809; MS (*m/z*): 216.0 $[M]^+$, 218.0 $[M+2]^+$.

5.1.1.4. N-(4-Fluorobenzyl)hydrazinecarbothioamide (34).

The intermediate (**34**) was synthesized as per the general Method A from 4-fluorobenzylamine (**14**) (1.0 g, 8.0 mmol) as white solid (Pervez et al., 2017). (Yield: 63%); m.p. 138–140 °C; IR (KBr, cm^{-1}): 3329, 3043, 2920, 1617, 1223, 1075; MS (*m/z*): 200.0 $[M+H]^+$.

5.1.1.5. N-(4-Methylbenzyl)hydrazinecarbothioamide (35).

The intermediate (**35**) was prepared according to the general Method A from 4-methylbenzylamine (**15**) (1.0 g, 8.26 mmol) as white solid (Pervez et al., 2017). (Yield: 65%); m.p. 154–156 °C; IR (KBr, cm^{-1}): 3322, 2918, 1616, 1270, 1075; MS (*m/z*): 195.75 $[M]^+$.

For intermediates (36–42) (Method B): To a stirred solution of substituted aniline (**16–22**) (1.0 equiv.) and NaOH (1.2 equiv.) in DMF (10 mL), a solution of carbon disulfide (1.2 equiv.) in DMF (5 mL) was gradually added and the resulting mixture was stirred for 3 h at RT. After complete consumption of starting material as checked by TLC, hydrazine hydrate (3.0 equiv.) was added to the above reaction mixture and it was heated to 70 °C for 1 h. After completion of the reaction as checked by TLC, the reaction mixture was allowed to cool to RT and diluted with cold water. The solid precipitates so obtained were filtered, washed with cold water and dried under reduced pressure to get the intermediate compounds (**36–42**).

5.1.1.6. N-Phenylhydrazinecarbothioamide (36).

The intermediate (**36**) was synthesized as per the general Method B from aniline (**16**) (1.0 g, 10.75 mmol) as white solid (Zhang et al., 2020). (Yield: 63%); m.p. 142–144 °C (lit m.p. 144–145 °C); IR (KBr, cm^{-1}): 3304, 3107, 1638, 1287, 1070.

5.1.1.7. N-(4-Methoxyphenyl)hydrazinecarbothioamide (37).

The intermediate (**37**) was synthesized as per the general Method B from 4-methoxyaniline (**17**) (1.0 g, 8.13 mmol) as white solid (Zhang et al., 2020). (Yield: 70%); m.p.

162–164 °C (lit m.p. 165–166 °C); IR (KBr, cm^{-1}): 3317, 3013, 2965, 1637, 1244, 1033.

5.1.1.8. **N-*(Pyridin-2-yl)hydrazinecarbothioamide (38).*** The intermediate (**38**) was synthesized as per the general Method B from 2-aminopyridine (**18**) (1.0 g, 10.63 mmol) as white solid (Aljahdali et al., 2014). (Yield: 65%); m.p. 188–190 °C (lit m.p. 193–194 °C); IR (KBr, cm^{-1}): 3241, 3029, 1607, 1207, 1008; MS (*m/z*): 169.0 $[M+H]^+$.

5.1.1.9. **N-*(5-Chloropyridin-2-yl)hydrazinecarbothioamide (39).*** The intermediate (**39**) was synthesized as per the general Method B from 2-amino-5-chloropyridine (**19**) (1.0 g, 7.81 mmol) as white solid (Sriram et al., 2009). (Yield: 63%); m.p. 112–114 °C; IR (KBr, cm^{-1}): 3243, 2997, 1609, 1203, 1014, 820; MS (*m/z*): 203.0 $[M]^+$, 205.0 $[M+2]^+$.

5.1.1.10. **N-*(5-Methylpyridin-2-yl)hydrazinecarbothioamide (40).*** The intermediate (**40**) was synthesized as per the general Method B from 2-amino-5-methylpyridine (**20**) (1.0 g, 9.25 mmol) as white solid. (Yield: 65%); m.p. 153–155 °C; IR (KBr, cm^{-1}): 3252, 3006, 1617, 1238, 1017; MS (*m/z*): 183.0 $[M+H]^+$.

5.1.1.11. **N-*(Pyrimidin-2-yl)hydrazinecarbothioamide (41).*** The intermediate (**41**) was synthesized as per the general Method B from 2-aminopyrimidine (**21**) (1.0 g, 10.52 mmol) as white solid (El-Masry, 2000). (Yield: 67%); m.p. 168–170 °C (lit m.p. 172 °C); IR (KBr, cm^{-1}): 3303, 3109, 1637, 1288, 1069.

5.1.1.12. **N-*(Pyrazin-2-yl)hydrazinecarbothioamide (42).*** The intermediate (**42**) was synthesized as per the general Method B from pyrazin-2-amine (**22**) (1.0 g, 10.52 mmol) as white solid. (Yield: 64%); m.p. 148–150°; IR (KBr, cm^{-1}): 3242, 3030, 1608, 1206, 1007.

5.1.2. N-(4-Chlorophenyl)hydrazinecarboxamide (43)

To a cold stirring solution of 4-chloroaniline (1.0 equiv.) and potassium carbonate (2.0 equiv.) in acetone (20 mL) at 0–5 °C, a solution of phenyl chloroformate (1.1 equiv.) in acetone (10 mL) was added gradually. After complete addition, the resulting reaction mixture was stirred at room temperature for additional 2 h. After completion of the reaction, the reaction mixture was concentrated *in vacuo*, quenched with 10% $NaHCO_3$ solution and diluted with cold water. The solid precipitates obtained were filtered and dried. The obtained solids were added to solution of hydrazine hydrate (3 equiv.) in 1,4-dioxane. The reaction mixture was heated to 100 °C for 4 h. After completion of the reaction as checked by TLC, the reaction mixture was allowed to cool to RT. The resulting precipitates were filtered and washed with ether to obtain the titled compound as white solid (Beukers et al., 2003). (Yield 75.2%); m.p. 188–190 °C (lit m.p. 190–192 °C); IR (KBr, cm^{-1}): 3334, 3230, 1670, 1142, 815.

5.1.3. General procedure for the synthesis of acyl hydrazide intermediates (44–50)

Method C. To a stirred solution of substituted benzoic acid/substituted phenylacetic acids/nicotinic acid (1 equiv.) in methanol (20 mL), conc. sulfuric acid in a catalytic amount was added. The resulting mixture was refluxed for 6 h. After completion of the reaction (confirmed by TLC), the mixture was concentrated to a volume of ~10 mL and partitioned between chloroform (30 mL) and water. The organic phase was washed with water, dried over anhydrous sodium sulfate and evaporated under reduced pressure to obtain liquid product. The resulting liquid was further added to a solution of hydrazine hydrate (3 equiv.) in methanol (20 mL). The reaction mixture was heated up to 65 °C for 4 h. After completion of the reaction as checked by TLC, the reaction mixture was allowed to cool to RT and the solid precipitates so obtained were filtered and washed with cold methanol to obtain the desired acyl hydrazides (**44**–**50**).

5.1.3.1. 2-Phenylacetohydrazide (44). The intermediate (**44**) was synthesized as per the general Method C from 2-phenylacetic acid (**24**) (1.0 g, 7.36 mmol) as white solid (Zimin et al., 2018). (Yield: 75%); m.p. 112–114 °C (lit m.p. 116–118 °C); IR (KBr, cm^{-1}): 3293, 3030, 1645, 1143.

5.1.3.2. 2-(4-Methoxyphenyl)acetohydrazide (45). The intermediate (**45**) was synthesized as per the general Method C from 2-(4-methoxyphenyl)acetic acid (**25**) (1.0 g, 7.35 mmol) as white solid (Hanif et al., 2012). (Yield: 75%); m.p. 128–130 °C (lit m.p. 126–127 °C); IR (KBr, cm^{-1}): 3341, 3030, 2957, 1619, 1107.

5.1.3.3. 2-(4-Chlorophenyl)acetohydrazide (46). The intermediate (**46**) was synthesized as per the general Method C from 2-(4-chlorophenyl)acetic acid (**26**) (1.0 g, 7.35 mmol) as white solid (Li et al., 2015). (Yield: 77%); m.p. 167–169 °C (lit m.p. 170–172 °C); IR (KBr, cm^{-1}): 3298, 3041, 1657, 1132, 850.

5.1.3.4. Benzohydrazide (47). The intermediate (**47**) was synthesized as per the general Method C from benzoic acid (**27**) (1.0 g, 7.35 mmol) as white solid (Saha et al., 2010). (Yield: 80%); m.p. 107–109 °C (lit m.p. 110–113 °C); IR (KBr, cm^{-1}): 3298, 3020, 1661, 1119.

5.1.3.5. 4-Fluorobenzohydrazide (48). The intermediate (**48**) was synthesized as per the general Method C from 4-fluorobenzoic acid (**28**) (1.0 g, 6.49 mmol) as white solid (Murty et al., 2016). (Yield: 79%); m.p. 162–164 °C (lit m.p. 161–163 °C); IR (KBr, cm^{-1}): 3302, 3017, 1664, 1119.

5.1.3.6. 4-Methylbenzohydrazide (49). The intermediate (**49**) was synthesized as per the general Method C from 4-methylbenzoic acid (**29**) (1.0 g, 6.66 mmol) as white solid (Saha et al., 2010). (Yield: 74%); m.p. 112–114 °C (lit m.p. 116–117 °C); IR (KBr, cm^{-1}): 3304, 3023, 1662, 1120.

5.1.3.7. Nicotinohydrazide (50). The intermediate (**50**) was synthesized as per the general Method C from nicotinic acid

(**30**) (1.0 g, 8.12 mmol) as white solid (Elif Öztürkkan Özbek et al., 2020). (Yield: 70%); m.p. 158–160 °C (lit m.p. 161–163 °C); IR (KBr, cm^{-1}): 3297, 3019, 1662, 1120.

5.1.4. 9-Ethyl-9*H*-carbazole (52)

To stirring solution of carbazole (**51**) (1.0 g, 6 mmol) in DMSO (15 mL), aqueous sodium hydroxide (0.48 g in 2 mL) solution was added, and the resulting reaction mixture was stirred for further 10 min. Ethyl iodide (0.6 mL, 7.06 mmol) was added in a dropwise manner to the above reaction mixture and it was allowed to stir at RT. TLC was used to monitor the progress of the reaction where after completion of the reaction, the reaction mixture was diluted with ice cold water and the solid so precipitated was collected by filtration, rinsed with cold water and dried in vacuum to yield the compound (**52**) as off white solid (Patel, Patel, Kanhed, Teli, Patel, Joshi, et al., 2020). (Yield: 1.07 g, 94%); m.p. 64–66 °C (lit m.p. 64–66 °C); IR (KBr, cm^{-1}): 3049, 2978, 2869, 1596, 1018, 753, 700; MS (*m/z*): 196.3 $[M+1]^+$.

5.1.5. 9-Ethyl-9*H*-carbazole-3-carbaldehyde (53)

Phosphoryl chloride (0.94 mL, 10.24 mmol) was added dropwise to an ice cooled stirred solution of ethyl carbazole (**52**) (2.0 g, 10.24 mmol) and dimethylformamide (0.76 mL, 10.24 mmol) in chloroform (20 mL) over a period of 10 min. After complete addition, the resulting reaction mixture was heated to reflux for 12–14 h. After completion of the reaction as checked by TLC, the reaction mixture was cooled to RT and then slowly diluted with ice cold water. The product was extracted using chloroform and washed with brine. The collected organic phase was washed with water, dried using anhydrous magnesium sulfate and concentrated under reduced pressure. The crude product so obtained was purified using column chromatography (eluent: 10% ethyl acetate in *n*-hexane) to afford the compound (**53**) as yellowish white solid (Patel, Patel, Kanhed, Teli, Patel, Joshi, et al., 2020). Yield 84%; m.p. 85–87 °C (lit m.p. 84–86 °C); IR (KBr, cm^{-1}): 3049, 2971, 2822, 2743, 1679, 1588, 620; ^{1}H NMR ($CDCl_3$): δ 10.12 (s, 1H, C*H*O), 8.64 (d, $J=2.0$ Hz, 1H, Ar*H*), 8.20–8.18 (m, 1H, Ar*H*), 8.05–8.03 (m, 1H, Ar*H*), 7.58–7.37 (m, 4H, Ar*H*), 4.43 (q, $J=7.2$ Hz, 2H, NCH_2CH_3), 1.50 (t, $J=7.2$ Hz, 3H, NCH_2CH_3); MS (*m/z*): 224.0 $[M+1]^+$.

5.1.6. General procedure for the synthesis of carbazole-based thiosemicarbazones (*54–65*), semicarbazone (*66*) and hydrazones (*67–73*)

Method D: A stirring reaction mixture of 9-ethyl-9*H*-carbazole-3-carbaldehyde (**53**) (0.25 g, 1.12 mmol) and appropiate thiosemicarbazides (**31**–**42**), semicarbazide (**43**) or acyl hydrazides (**44**–**50**) (1.1 equiv.) with acetic acid (0.1 mL) in methanol (20 mL) was heated to reflux for 4–5 h. After completion of reaction, the reaction mixture was allowed to cool to RT. After standing for 2 h, the crystalline solid so formed was collected by vaccum filtration and rinsed with methanol to obtain the desired compounds (**54**–**73**).

5.1.6.1. (E)-N-*Benzyl-2-((9-ethyl-9H-carbazol-3-yl)methylene)hydrazinecarbothioamide (54).*

Compound (**54**) was synthesized as per the general Method D from the intermediates (**53**) (1.0 g, 4.46 mmol) and (**31**) (0.89 g, 4.93 mmol) as a white solid. (Yield: 75%); m.p. 128–129 °C; IR (KBr, cm^{-1}): 3359, 3058, 2973, 1595, 1231, 1074; ^{1}H NMR ($CDCl_3$): δ 9.30 (s, 1H, -N*H*CSNH), 8.28 (s, 1H, Ar*H*), 8.09 (d, $J=7.5$ Hz, 1H, Ar*H*), 7.96 (s, 1H, -C*H*N), 7.80 (t, $J=6.0$ Hz, 1H, -NHCSN*H*), 7.76–7.74 (dd, $J=8.5$ Hz, 2.0 Hz, 1H, Ar*H*), 7.51–7.36 (m, 7H, Ar*H*), 7.33–7.24 (m, 2H, Ar*H*), 5.03 (d, $J=6.0$ Hz, 2H, $NHCH_2$), 4.39–4.34 (q, $J=7.5$ Hz, 2H, NCH_2CH_3), 1.43 (t, $J=7.5$ Hz, 3H, NCH_2CH_3); MS (*m/z*): 387.0 $[M+1]^+$.

5.1.6.2. (E)-N-*(4-Methoxybenzyl)-2-((9-ethyl-9H-carbazol-3-yl)methylene)hydrazine carbothioamide (55).*

Compound (**55**) was synthesized as per the general Method D from the intermediates (**53**) (1.0 g, 4.46 mmol) and (**32**) (1.04 g, 4.93 mmol) as a white solid. (yield: 81%); m.p. 180–181 °C; IR (KBr, cm^{-1}): 3297, 3058, 2988, 1592, 1232, 1064; ^{1}H NMR ($CDCl_3$): δ 9.28 (s, 1H, -N*H*CSNH), 8.26 (d, $J=1.5$ Hz, 1H, Ar*H*), 8.09 (d, $J=8.0$ Hz, 1H, Ar*H*), 7.96 (s, 1H, -C*H*N), 7.75–7.71 (m, 1H, -NHCSN*H*; m, 1H, Ar*H*), 7.51–7.47 (m, 1H, Ar*H*), 7.42–7.36 (m, 4H, Ar*H*), 7.27–7.24 (m, 1H, Ar*H*), 6.93–6.90 (m, 2H, Ar*H*), 4.94 (d, $J=6.0$ Hz, 2H, $NHCH_2$), 4.38–4.34 (q, $J=7.5$ Hz, 2H, NCH_2CH_3), 3.80 (s, 3H, OCH_3), 1.43 (t, $J=7.5$ Hz, 3H, NCH_2CH_3); MS (*m/z*): 417.0 $[M+1]^+$.

5.1.6.3. (E)-N-*(4-Chlorobenzyl)-2-((9-ethyl-9H-carbazol-3-yl)methylene)hydrazinecarbo thioamide (56).*

Compound (**56**) was synthesized as per the general Method D from the intermediates (**53**) (1.0 g, 4.46 mmol) and (**33**) (1.05 g, 4.93 mmol) as a white solid. (Yield: 79%); m.p. 208–210 °C; IR (KBr, cm^{-1}): 3347, 2977, 1596, 1228, 1093, 801; ^{1}H NMR ($CDCl_3$): δ 9.31 (s, 1H, -N*H*CSNH), 8.28 (d, $J=1.5$ Hz, 1H, Ar*H*), 8.09 (d, $J=8.0$ Hz, 1H, Ar*H*), 7.97 (s, 1H, -C*H*N), 7.80 (t, $J=6.0$ Hz, 1H, -NHCSN*H*), 7.76–7.74 (dd, $J=8.5$ Hz, 1.5 Hz, 1H, Ar*H*), 7.51–7.48 (m, 1H, Ar*H*), 7.43–7.32 (m, 5H, Ar*H*), 7.28–7.25 (m, 2H, Ar*H*), 4.99 (d, $J=6.0$ Hz, 2H, $NHCH_2$), 4.39–4.34 (q, $J=7.5$ Hz, 2H, NCH_2CH_3), 1.43 (t, $J=7.5$ Hz, 3H, NCH_2CH_3); ^{13}C NMR ($CDCl_3$): δ 177.4, 144.8, 141.3, 140.4, 136.4, 133.4, 129.1, 128.8, 126.4, 124.8, 123.9, 123.2, 122.7, 120.7, 120.6, 119.7, 108.9, 108.8, 47.4, 37.7, 13.8; MS (*m/z*): 421.0 $[M]^+$, 423.0 $[M+2]^+$.

5.1.6.4. (E)-N-*(4-Fluorobenzyl)-2-((9-ethyl-9H-carbazol-3-yl)methylene)hydrazinecarbo thioamide (57).*

Compound (**57**) was synthesized as per the general Method D from the intermediates (**53**) (1.0 g, 4.46 mmol) and (**34**) (0.98 g, 4.93 mmol) as a white solid. (Yield: 80%); m.p. 195–197 °C; IR (KBr, cm^{-1}): 3354, 3062, 3002, 1598, 1215, 1091, 941; ^{1}H NMR ($CDCl_3$): δ 9.42 (s, 1H, -N*H*CSNH), 8.28 (d, $J=1.5$ Hz, 1H, Ar*H*), 8.09 (d, $J=8.0$ Hz, 1H, Ar*H*), 7.98 (s, 1H, -C*H*N), 7.78 (t, $J=6.0$ Hz, 1H, -NHCSN*H*), 7.76–7.74 (dd, $J=8.5$ Hz, 1.5 Hz, 1H, Ar*H*), 7.51–7.48 (m, 1H, Ar*H*), 7.43–7.37 (m, 4H, Ar*H*), 7.28–7.25 (m, 1H, Ar*H*), 7.08-7.04 (m, 2H, Ar*H*), 4.99 (d, $J=6.0$ Hz, 2H, $NHCH_2$), 4.38-4.34 (q, $J=7.5$ Hz, 2H,

-NHCH_2CH$_3$), 1.43 (t, $J = 7.5$ Hz, 3H, -NHCH$_2$CH_3); MS (*m/z*): 405.0 $[M + 1]^+$.

5.1.6.5. (E)-N-(4-Methylbenzyl)-2-((9-ethyl-9H-carbazol-3-yl)methylene)hydrazinecarbo thioamide (58). Compound (**58**) was synthesized as per the general Method D from the intermediates (**53**) (1.0 g, 4.46 mmol) and (**35**) (0.82 g, 4.93 mmol) as a white solid. (Yield: 84%). m.p. 210–212 °C; IR (KBr, cm^{-1}): 3361, 3054, 3003, 1594, 1233, 1123; ^{1}H NMR (CDCl$_3$): δ 9.13 (s, 1H, -N*H*CSNH), 8.27 (d, $J = 1.5$ Hz, 1H, Ar*H*), 8.09 (d, $J = 7.5$ Hz, 1H, Ar*H*), 7.94 (s, 1H, -C*H*N), 7.76–7.74 (m, 1H, -NHCSN*H*; m, 1H, Ar*H*), 7.51–7.48 (m, 1H, Ar*H*), 7.43–7.33 (m, 4H, Ar*H*), 7.28–7.24 (m, 2H, Ar*H*), 7.19 (d, $J = 8.0$ Hz, 1H, Ar*H*), 4.97 (d, $J = 5.5$ Hz, 2H, -NHCH_2), 4.39–4.34 (q, $J = 7.5$ Hz, 2H, -NCH_2CH$_3$), 2.36 (s, 3H, ArCH_3), 1.43 (t, $J = 7.5$ Hz, 3H, -NCH$_2$CH_3); ^{13}C NMR (CDCl$_3$): δ 177.2, 144.4, 141.3, 140.4, 137.3, 134.7, 129.4, 127.8, 126.3, 124.8, 124.0, 123.2, 122.7, 120.7, 120.6, 119.6, 108.8, 108.8, 48.1, 37.7, 21.1, 13.8; MS (*m/z*): 401.0 $[M + 1]^+$.

5.1.6.6. (E)-2-((9-Ethyl-9H-carbazol-3-yl)methylene)-N-phenylhydrazinecarbothioamide (59). Compound (**59**) was synthesized as per the general Method D from the intermediates (**53**) (1.0 g, 4.46 mmol) and (**36**) (0.82 g, 4.93 mmol) as a white solid. (Yield: 85%). m.p. 207–209 °C; IR (KBr, cm^{-1}): 3242, 3047, 2977, 1596, 1202, 1073; ^{1}H NMR (CDCl$_3$): δ 9.97 (s, 1H, -N*H*CSNH), 9.28 (s, 1H, -NHCSN*H*), 8.34 (s, 1H, Ar*H*), 8.13 (d, $J = 7.5$ Hz, 1H, Ar*H*), 8.09 (s, 1H, -C*H*N), 7.84–7.82 (dd, $J = 7.5$ Hz, 2.0 Hz, 1H, Ar*H*), 7.71 (d, $J = 7.5$ Hz, 2H, Ar*H*), 7.52–7.40 (m, 5H, Ar*H*), 7.29–7.25 (m, 2H, Ar*H*), 4.40–4.35 (q, $J = 7.5$ Hz, 2H, -NCH_2CH$_3$), 1.45 (t, $J = 7.5$ Hz, 3H, -NCH$_2$CH_3); MS (*m/z*): 373.0 $[M + 1]^+$.

5.1.6.7. (E)-2-((9-Ethyl-9H-carbazol-3-yl)methylene)-N-(4-methoxyphenyl)hydrazine carbothioamide (60). Compound (**60**) was synthesized as per the general Method D from the intermediates (**53**) (1.0 g, 4.46 mmol) and (**37**) (0.97 g, 4.93 mmol) as a white solid. (Yield: 82%); m.p. 223–225 °C; IR (KBr, cm^{-1}): 3331, 3043, 2977, 1595, 1236, 1067; ^{1}H NMR (CDCl$_3$): δ 9.20 (s, 1H, -N*H*CSNH), 9.10 (s, 1H, -NHCSN*H*), 8.36 (d, $J = 1.5$ Hz, 1H, Ar*H*), 8.13 (d, $J = 8$ Hz, 1H, Ar*H*), 8.00 (s, 1H, -C*H*N), 7.84–7.82 (m, 1H, Ar*H*), 7.54–7.49 (m, 3H, Ar*H*), 7.45–7.42 (m, 2H, Ar*H*), 7.29–7.25 (m, 1H, Ar*H*), 6.96–6.94 (m, 2H, Ar*H*), 4.41–4.37 (q, $J = 7.5$ Hz, 2H, -NCH_2CH$_3$), 3.84 (s, 3H, -OCH_3), 1.46 (t, $J = 7.5$ Hz, 3H, -NCH$_2$CH_3); MS (*m/z*): 403.0 $[M + 1]^+$.

5.1.6.8. (E)-2-((9-Ethyl-9H-carbazol-3-yl)methylene)-N-(pyridin-2-yl)hydrazinecarbo thioamide (61). Compound (**61**) was synthesized as per the general Method D from the intermediates (**53**) (1.0 g, 4.46 mmol) and (**38**) (0.82 g, 4.93 mmol) as a white solid. (Yield: 83%); m.p. 198–201 °C; IR (KBr, cm^{-1}): 3228, 3041, 2968, 1602, 1236, 1144; ^{1}H NMR (CDCl$_3$): δ 9.91 (s, 1H, -NHCSN*H*), 9.35 (s, 1H, -N*H*CSNH), 8.95 (d, $J = 8.0$ Hz, 1H, Ar*H*), 8.44–8.37 (m, 2H, Ar*H*), 8.15 (d, $J = 7.5$ Hz, 1H, Ar*H*), 8.02 (s, 1H, -C*H*N), 7.92–7.90 (dd, $J = 8.5$ Hz, 1.5 Hz, 1H, Ar*H*), 7.78–7.75 (m, 1H, Ar*H*), 7.52–7.49 (m, 1H, Ar*H*), 7.44–7.40 (m, 2H, Ar*H*), 7.30–7.25 (m, 1H, Ar*H*), 7.13–7.10 (m, 1H, Ar*H*), 4.40–4.36 (q, $J = 7.5$ Hz, 2H, -NCH_2CH$_3$), 1.45 (t, $J = 7.5$ Hz, 3H, -NCH$_2$CH_3); ^{13}C NMR (CDCl$_3$): δ 173.7, 151.7, 148.0, 144.9, 141.5, 140.4, 137.7, 126.4, 125.1, 123.5, 123.3, 122.7, 121.1, 120.8, 120.3, 119.7, 118.1, 115.4, 108.9, 37.8, 13.8; MS (*m/z*): 374.0 $[M + 1]^+$.

5.1.6.9. (E)-2-((9-Ethyl-9H-carbazol-3-yl)methylene)-N-(5-chloropyridin-2-yl)hydrazine carbothioamide (62). Compound (**62**) was synthesized as per the general Method D from the intermediates (**53**) (1.0 g, 4.46 mmol) and (**39**) (0.99 g, 4.93 mmol) as a white solid. (Yield: 81%); m.p. 204–206 °C; IR (KBr, cm^{-1}): 3311, 3050, 2974, 1597, 1236, 1119, 753; ^{1}H NMR (CDCl$_3$): δ 9.90 (s, 1H, -NHCSN*H*), 9.20 (s, 1H, -N*H*CSNH), 8.97 (d, $J = 9.0$ Hz, 1H, Ar*H*), 8.36 (s, 1H, Ar*H*), 8.33 (d, $J = 3$ Hz, 1H, Ar*H*), 8.16–8.14 (dd, $J = 9.0$ Hz, 1.0 Hz, 1H, Ar*H*), 8.01 (s, 1H, -C*H*N), 7.90 (d, $J = 8.5$ Hz, 1H, Ar*H*), 7.72–7.70 (dd, $J = 9.0$ Hz, $J = 3.0$ Hz, 1H, Ar*H*), 7.53–7.50 (m, 1H, Ar*H*), 7.45–7.42 (m, 2H, Ar*H*), 7.31–7.25 (m, 1H, Ar*H*), 4.41–4.37 (q, $J = 7.5$ Hz, 2H, -NCH_2CH$_3$), 1.46 (t, $J = 7.5$ Hz, 3H, -NCH$_2$CH_3); ^{13}C NMR (CDCl$_3$): δ 173.4, 150.0, 146.6, 145.3, 141.6, 140.4, 137.2, 127.3, 126.4, 125.0, 123.4, 123.3, 122.7, 121.2, 120.7, 119.8, 115.9, 109.0, 108.9, 37.8, 13.8; MS (*m/z*): 408 $[M]^+$, 410 $[M + 2]^+$.

5.1.6.10. (E)-2-((9-Ethyl-9H-carbazol-3-yl)methylene)-N-(5-methylpyridin-2-yl)hydra- zinecarbothioamide (63). Compound (**63**) was synthesized as per the general Method D from the intermediates (**53**) (1.0 g, 4.46 mmol) and (**40**) (0.89 g, 4.93 mmol) as a white solid. (Yield: 79%); m.p. 173–176 °C; IR (KBr, cm^{-1}): 3278, 3019, 2973, 1594, 1234, 1070; ^{1}H NMR (CDCl$_3$): δ 9.86 (s, 1H, -NHCSN*H*), 9.26 (s, 1H, -N*H*CSNH), 8.76 (d, $J = 8.0$ Hz, 1H, Ar*H*), 8.39 (d, $J = 2.0$ Hz, 1H, Ar*H*), 8.21 (d, $J = 2.0$ Hz, 1H, Ar*H*), 8.16 (d, $J = 8.0$ Hz, 1H, Ar*H*), 8.00 (s, 1H, -C*H*N), 7.93–7.91 (m, 1H, Ar*H*), 7.59–7.57 (m, 1H, Ar*H*), 7.52–7.49 (m, 1H, Ar*H*), 7.44–7.41 (m, 2H, Ar*H*), 7.30–7.25 (m, 1H, Ar*H*), 4.41–4.37 (q, $J = 7.5$ Hz, 2H, -NCH_2CH$_3$), 2.10 (s, 3H, ArCH_3), 1.46 (t, $J = 7.5$ Hz, 3H, -NCH$_2$CH_3); MS (*m/z*): 388.0 $[M + 1]^+$.

5.1.6.11. (E)-2-((9-Ethyl-9H-carbazol-3-yl)methylene)-N-(pyrimidin-2-yl)hydrazine carbothioamide (64). Compound (**64**) was synthesized as per the general Method D from the intermediates (**53**) (1.0 g, 4.46 mmol) and (**41**) (0.83 g, 4.93 mmol) as a white solid. (Yield: 78%); m.p. 87–89 °C; IR (KBr, cm^{-1}): 3055, 2972, 1587, 1233, 1143; ^{1}H NMR (CDCl$_3$): δ 10.08 (s, 1H, -NHCSN*H*), 8.60 (s, 1H, -N*H*CSNH), 8.14 (d, 1H, -C*H*N, 1H, Ar*H*), 8.01–7.99 (m, 1H, Ar*H*), 7.54–7.51 (m, 2H, Ar*H*), 7.47–7.44 (m, 4H, Ar*H*), 7.33–7.30 (m, 2H, Ar*H*), 4.41–4.37 (q, $J = 7.5$ Hz, 2H, -NCH_2CH$_3$), 1.46 (t, $J = 7.5$ Hz, 3H, -NCH$_2$CH_3); MS (*m/z*) 375.4 $[M + 1]^+$.

5.1.6.12. (E)-2-((9-Ethyl-9H-carbazol-3-yl)methylene)-N-(pyrazin-2-yl)hydrazinecarbo thioamide (65). Compound (**65**) was synthesized as per the general Method D from the intermediates (**53**) (1.0 g, 4.46 mmol) and (**42**) (0.83 g, 4.93 mmol) as a white solid. (Yield: 81%); m.p. 88–90 °C; IR (KBr, cm^{-1}): 3054, 2971, 1586, 1233, 1143; ^{1}H NMR (CDCl$_3$): δ 10.08 (s, 1H, -NHCSN*H*), 8.59 (s, 1H, -N*H*CSNH), 8.15–8.13 (m,

1H, -C*H*N, 1H, Ar*H*), 8.01–7.99 (m, 1H, Ar*H*), 7.54–7.51 (m, 2H, Ar*H*), 7.47–7.44 (m, 4H, Ar*H*), 7.33–7.30 (m, 2H, Ar*H*), 4.40–4.36 (q, $J = 7.5$ Hz, 2H, -NCH_2CH$_3$), 1.45 (t, $J = 7.5$ Hz, 3H, -NCH$_2$CH_3); MS (*m/z*): 374.0 $[M]^+$.

5.1.6.13. (E)-N-(4-Chlorophenyl)-2-((9-ethyl-9H-carbazol-3-yl)methylene)hydrazine carboxamide (66). Compound (**66**) was synthesized as per the general Method D from the intermediates (**53**) (1.0 g, 4.46 mmol) and (**43**) (0.91 g, 4.93 mmol) as a white solid. (Yield: 75%); m.p. 251–253 °C; IR (KBr, cm^{-1}): 3322, 3061, 2973, 1672, 1593, 1133, 742; ^{1}H NMR (CDCl$_3$): δ 8.32 (s, 1H, -N*H*CONH), 8.20 (s, 1H, -NHCON*H*), 8.14 (d, $J = 7.5$ Hz, 1H, Ar*H*), 7.91 (s, 1H, -C*H*N), 7.90 (d, 1H, Ar*H*), 7.83–7.81 (m, 1H, Ar*H*), 7.56–7.50 (m, 3H, Ar*H*), 7.44 (d, 2H, Ar*H*), 7.32–7.25 (m, 3H, Ar*H*), 4.42–4.38 (q, $J = 7.5$ Hz, 2H, -NCH_2CH$_3$), 1.46 (t, $J = 7.5$ Hz, 3H, -NCH$_2$CH_3); ^{13}C NMR (DMSO-d_6): δ 153.0, 142.2, 140.2, 139.9, 138.2, 128.1, 126.0, 125.7, 125.2, 124.8, 122.2, 122.1, 121.1, 120.5, 119.7, 119.1, 109.3, 109.1, 37.01, 13.6; MS (*m/z*): 391.0 $[M]^+$, 393.0 $[M + 2]^+$.

5.1.6.14. (E)-N′-((9-Ethyl-9H-carbazol-3-yl)methylene)-2-phenylacetohydrazide (67). Compound (**67**) was synthesized as per the general Method D from the intermediates (**53**) (1.0 g, 4.46 mmol) and (**44**) (0.73 g, 4.93 mmol) as a white solid. (Yield: 80%). m.p. 237–239 °C; IR (KBr, cm^{-1}): 3170, 3021, 2931, 1651, 1597, 1149; ^{1}H NMR (CDCl$_3$): δ 8.67 (s, 1H, -N*H*CO), 8.31 (d, $J = 1.5$ Hz, 1H, Ar*H*), 8.13 (d, $J = 7.5$ Hz, 1H, Ar*H*), 7.88 (s, 1H, -C*H*N), 7.87–7.85 (m, 1H, Ar*H*), 7.52–7.41 (m, 5H, Ar*H*), 7.37–7.25 (m, 4H, Ar*H*), 4.42–4.37 (q, $J = 7.5$ Hz, 2H, -NCH_2CH$_3$), 4.16 (s, 2H, -COCH_2), 1.46 (t, $J = 7.5$ Hz, 3H, -NCH$_2$CH_3); MS (*m/z*): 356.0 $[M + 1]^+$.

5.1.6.15. (E)-N′-((9-Ethyl-9H-carbazol-3-yl)methylene)-2-(4-methoxyphenyl)aceto hydrazide (68). Compound (**68**) was synthesized as per the general Method D from the intermediates (**53**) (1.0 g, 4.46 mmol) and (**45**) (0.88 g, 4.93 mmol) as a white solid. (Yield: 79%); m.p. 214–217 °C; IR (KBr, cm^{-1}): 3170, 3017, 2970, 1645, 1598, 1263, 1151; ^{1}H NMR (CDCl$_3$): δ 8.80 (s, 1H, -N*H*CO), 8.32 (d, $J = 1.5$ Hz, 1H, Ar*H*), 8.13 (d, $J = 7.5$ Hz, 1H, Ar*H*), 7.89 (s, 1H, -C*H*N), 7.88–7.86 (dd, $J = 1.5$ Hz, 8.5 Hz, 1H, Ar*H*), 7.52–7.49 (m, 1H, Ar*H*), 7.43 (d, $J = 8$ Hz, 2H, Ar*H*), 7.35 (d, $J = 8.5$ Hz, 2H, Ar*H*), 7.29–7.25 (m, 3H, Ar*H*), 4.42–4.37 (q, $J = 7.5$ Hz, 2H, -NCH_2CH$_3$), 4.10 (s, 2H, -COCH_2), 3.77 (s, 3H, -OCH_3), 1.46 (t, $J = 7.5$ Hz, 3H, -NCH$_2$CH_3); MS (*m/z*): 386.0 $[M + 1]^+$.

5.1.6.16. (E)-N′-((9-Ethyl-9H-carbazol-3-yl)methylene)-2-(4-chlorophenyl)aceto hydrazide (69). Compound (**69**) was synthesized as per the general Method D from the intermediates (**53**) (1.0 g, 4.46 mmol) and (**46**) (0.90 g, 4.93 mmol) as a white solid. (Yield: 83%); m.p. 239–241 °C; IR (KBr, cm^{-1}): 3311, 3106, 2967, 1672, 1599, 1129; ^{1}H NMR (CDCl$_3$): δ 8.64 (s, 1H, -N*H*CO), 8.31 (d, $J = 1.5$ Hz, 1H, Ar*H*), 8.12 (d, $J = 7.5$ Hz, 1H, Ar*H*), 7.89 (s, 1H, -C*H*N), 7.86–7.84 (dd, $J = 8.5$ Hz, 1.5 Hz, 1H, Ar*H*), 7.52–7.49 (m, 1H, Ar*H*), 7.45–7.43 (m, 2H, Ar*H*), 7.36 (d, $J = 8.5$ Hz, 2H, Ar*H*), 7.31–7.25 (m, 3H, Ar*H*), 4.42–4.38 (q, $J = 7.5$ Hz, 2H, -NCH_2CH$_3$), 4.13 (s, 2H, -COCH_2), 1.46 (t, $J = 7.5$ Hz, 3H, -NCH$_2$CH_3); MS (*m/z*): 390.0 $[M]^+$, 392.0 $[M + 2]^+$.

5.1.6.17. (E)-N′-((9-Ethyl-9H-carbazol-3-yl)methylene)benzohydrazide (70). Compound (**70**) was synthesized as per the general Method D from the intermediates (**53**) (1.0 g, 4.46 mmol) and (**47**) (0.67 g, 4.93 mmol) as a white solid. (Yield: 77%); m.p. 229–231 °C; IR (KBr, cm^{-1}): 3177, 3015, 2978, 1639, 1599, 1143; ^{1}H NMR (CDCl$_3$): δ 9.13 (s, 1H, -N*H*CO), 8.51 (s, 1H, Ar*H*), 8.41 (s, 1H, -C*H*N), 8.11 (d, $J = 8.0$ Hz, 1H, Ar*H*), 7.94 (d, $J = 8.5$ Hz, 1H, Ar*H*), 7.88 (d, $J = 7.5$ Hz, 1H, Ar*H*), 7.57–7.54 (m, 1H, Ar*H*), 7.51–7.47 (m, 4H, Ar*H*), 7.42–7.40 (m, 2H, Ar*H*), 7.27–7.25 (m, 1H, Ar*H*), 4.39–4.35 (q, $J = 7.5$ Hz, 2H, -NCH_2CH$_3$), 1.44 (t, $J = 7.5$ Hz, 3H, -NCH$_2$CH_3); ^{13}C NMR (DMSO-d_6): δ 162.8, 148.9, 140.5, 139.9, 133.6, 131.4, 128.3, 127.4, 126.1, 125.2, 124.5, 122.2, 122.0, 120.5, 120.0, 119.2, 109.4, 109.3, 37.01, 13.6; MS (*m/z*): 342.0 $[M + 1]^+$.

5.1.6.18. (E)-N′-((9-Ethyl-9H-carbazol-3-yl)methylene)-4-fluorobenzohydrazide (71). Compound (**71**) was synthesized as per the general Method D from the intermediates (**53**) (1.0 g, 4.46 mmol) and (**48**) (0.75 g, 4.93 mmol) as a white solid. (Yield: 82%); m.p. 232–235 °C; IR (KBr, cm^{-1}): 3186, 3016, 2978, 1644, 1599, 1150; ^{1}H NMR (CDCl$_3$): δ 9.06 (s, 1H, -N*H*CO), 8.50 (s, 1H, Ar*H*), 8.41 (s, 1H, -C*H*N), 8.12 (d, $J = 7.0$ Hz, 1H, Ar*H*), 7.91 (s, 2H, Ar*H*), 7.51–7.48 (m, 1H, Ar*H*), 7.43–7.40 (m, 2H, Ar*H*), 7.28–7.24 (m, 3H, Ar*H*), 7.19–7.16 (m, 1H, Ar*H*), 4.40–4.35 (q, $J = 7.5$ Hz, 2H, -NCH_2CH$_3$), 1.44 (t, $J = 7.5$ Hz, 3H, -NCH$_2$CH_3); MS (*m/z*): 360.0 $[M + 1]^+$.

5.1.6.19. (E)-N′-((9-Ethyl-9H-carbazol-3-yl)methylene)-4-methylbenzohydrazide (72). Compound (**72**) was synthesized as per the general Method D from the intermediates (**53**) (1.0 g, 4.46 mmol) and (**49**) (0.73 g, 4.93 mmol) as a white solid. (Yield: 85%); m.p. 252–254 °C; IR (KBr, cm^{-1}): 3181, 3030, 2979, 1640, 1554, 1145; ^{1}H NMR (CDCl$_3$): δ 9.04 (s, 1H, -N*H*CO), 8.51 (s, 1H, Ar*H*), 8.40 (s, 1H, -C*H*N), 8.12 (d, $J = 8.0$ Hz 1H, Ar*H*), 7.93 (d, $J = 9.0$ Hz 1H, Ar*H*), 7.78 (d, $J = 7.0$ Hz, 1H, Ar*H*), 7.50–7.47 (m, 1H, Ar*H*), 7.43–7.40 (m, 3H, Ar*H*), 7.30–7.25 (m, 3H, Ar*H*), 4.40-4.36 (q, $J = 7.0$ Hz, 2H, -NCH_2CH$_3$), 2.43 (s, 3H, ArCH_3), 1.45 (t, $J = 7.0$ Hz, 3H, -NCH$_2$CH_3); ^{13}C NMR (DMSO-d_6): δ 162.6, 148.6, 141.4, 140.5, 139.9, 130.7, 128.8, 127.4, 126.1, 125.2, 124.4, 122.2, 122.0, 120.5, 119.9, 119.2, 109.7, 109.4, 109.3, 37.05, 20.9, 13.6; MS (*m/z*): 356.0 $[M + 1]^+$.

5.1.6.20. (E)-N′-((9-Ethyl-9H-carbazol-3-yl)methylene)picolinoylhydrazide (73). Compound (**73**) was synthesized as per the general Method D from the intermediates (**53**) (1.0 g, 4.46 mmol) and (**50**) (0.74 g, 4.93 mmol) as a white solid. (Yield: 76%); m.p. 212–216 °C; IR (KBr, cm^{-1}): 3178, 3009, 2978, 1637, 1597, 1148; ^{1}H NMR (CDCl$_3$): δ 9.90 (s, 1H, -N*H*CO), 8.77–8.73 (m, 1H, Ar*H*), 8.42 (s, 1H, -C*H*N), 8.26–8.23 (m, 1H, Ar*H*), 8.08–8.03 (m, 2H, Ar*H*), 7.90–7.88 (m, 1H, Ar*H*), 7.47–7.32 (m, 5H, Ar*H*), 7.25–7.20 (m, 1H, Ar*H*), 4.36–4.28 (m, 2H, -NCH_2CH$_3$), 1.42–1.37 (m, 3H, -NCH$_2$CH_3); MS (*m/z*): 343.0 $[M + 1]^+$.

5.2. Biology

5.2.1. In vitro *ChE* inhibition studies

The potential of the test compounds to inhibit ChEs was assessed using Ellman's method as reported in our earlier publications (Kanhed, Patel, Patel, et al., 2020; Patel, Patel, Kanhed, Teli, Patel, Gandhi, et al., 2020). Tacrine and donepezil were used as the standard drugs for the study. The absorbance values at different concentrations of the test compounds and the standard drugs were used to calculate the IC_{50} values of the respective compounds.

5.2.2. DPPH radical scavenging activity

The potential of the test compounds to scavenge the DPPH radical was evaluated by DPPH spectrophotometric assay as described in our previous reports (Patel et al., 2019, Patel, Patel, Kanhed, Teli, Patel, Gandhi, et al., 2020). The quantification of free radical scavenging activity of the test compounds was done in the form of reduction percentage (RP) of DPPH calculated by the equation $RP = 100[(A_0 - A_C)/A_0]$, where A_0 is the absorbance of DPPH without sample and A_C is the absorbance after adding sample with concentration C. Here, ascorbic acid was taken as a positive control (Kedare & Singh, 2011).

5.2.3. Metal chelation study

The tendency of the selected test compounds to form chelates with the biometals was evaluated using UV spectrophotometry as detailed in our earlier report (Patel, Patel, Kanhed, Teli, Patel, Joshi, et al., 2020). The UV absorption spectra of the test compounds (**61** and **62**) and 8-hydroxyquinoline (reference compound) were recorded alone and in the presence of $CuSO_4$, $FeCl_3$, $FeSO_4$, $ZnCl_2$, $AlCl_3$, $CaCl_2$ or $MgSO_4$ with wavelengths ranging from 200 to 600 nm after incubating the solutions for 30 min. in methanol at room temperature. Final concentration of the test compounds and the reference compound was 25 μM.

5.3. Computational studies

5.3.1. Docking studies of compounds (61 and 62) with ChEs

Docking studies were performed using Glide module of Schrodinger Suite (Schrödinger 2009, LLC, New York, NY). The protein structures of AChE (PDB code: 2CKM, 1B41) and BuChE (PDB code: 4BDS) were obtained from the RCSB Protein Data Bank and checked for structural correctness with Protein Preparation Wizard of Schrodinger using OPLS force field. The grids were generated on the active sites of the respective protein structures. The generated grids were validated by redocking of the knocked out co-crystallised ligands into the active sites of the grids. The redocked ligands showed similar interactions as shown by the original co-crystallized ligands. The grids were validated by comparing the RMSD values of the redocked ligands with the co-crystallized ligands present in 2CKM and 4BDS and the values obtained were 0.40 and 0.26 A, respectively. The 3D structures of **61** and **62** were built with the Build module within Maestro, and conformational search was carried out using OPLS force field at physiological pH with the LigPrep module of Schrödinger. Docking studies were conducted in extra-precision (XP) mode where extensive conformational search is carried out to identify the suitable binding conformation which can bind within the receptor active site.

5.3.2. Molecular dynamics simulation

The MD analyses were carried out for 50 ns time duration by using GROMACS 2020.1 tool (GROMACS 2020). MD protocol was followed as reported previously by our group (Kanhed, Patel, Patel, et al., 2020).

5.3.3. In silico prediction of ADMET properties

Prediction of *in silico* ADMET properties was performed using the QikProp module of Schrodinger Suite and pkCSM web tool. The ligand structures built for the docking studies were used for the prediction of the different ADMET descriptors. The significant descriptors examined are presented in this report.

5.3.4. Prediction of site of metabolism by SMARTCyp

SMARTCyp, a SOM predicting software released by Rydberg et al. contains a database of compounds metabolized by CYP450 with precalculated density functional theory (DFT) activation energies (Rydberg, Gloriam, & Olsen, 2010; Rydberg, Gloriam, Zaretzki et al., 2010). To rank the SOM, SMARTCyp uses database having SMiles ARbitrary Target Specification-based fragments in combination with an accessibility descriptor. The test ligands were uploaded as SMILES strings format representing the molecule. The obtained results included the molecular structure and an atom ranking table for each ligand. Three top-ranked atoms were highlighted in the structure as well as in the table, as shown in Figure 5.

Disclosures statement

The authors declare that there are no conflicts of interest.

Funding

Kishan B. Patel is thankful to the AICTE, New Delhi for awarding PG Scholarship (GPAT) [ID-1-3526872437]. Dushyant V. Patel greatly acknowledges the DST-INSPIRE, New Delhi for awarding Research Fellowship (IF-150660).

Author contributions

M.R.Y. conceptualized the whole study. K.B.P., D.V.P. and N.R.P. carried out synthesis and data collection. A.M.K. planned and executed the computational studies. B.G. and B.S.S. assisted in synthesis and data collection. K.V.P. designed the biological studies. B.N.C. and K.B.P. performed biological studies and data collection. N.K.P. and D.M.T.

helped in the synthesis and data interpretation. K.B.P. and D.V.P. drafted the manuscript. All authors reviewed and approved the final version of the manuscript.

References

Aljahdali, M. S., Elmalik, Y. H., & El-Reash, G. M. A. (2014). Synthesis of some transition metal complexes of novel 1-methylpyrazole-3-aldehyde-4-(2-pyridyl)thiosemicarbazone: Spectroscopic and in vitro biological activity studies. *European Journal of Chemistry*, *5*(2), 201–208. https://doi.org/10.5155/eurjchem.5.2.201-208.952

Bajda, M., Guzior, N., Ignasik, M., & Malawska, B. (2011). Multi-target-directed ligands in Alzheimer's disease treatment. *Current Medicinal Chemistry*, *18*(32), 4949–4975. https://doi.org/10.2174/092986711797535245

Bertini, S., Ghilardi, E., Asso, V., Minutolo, F., Rapposelli, S., Digiacomo, M., Saccomanni, G., Salmaso, V., Sturlese, M., Moro, S., Macchia, M., & Manera, C. (2017). Sulfonamido-derivatives of unsubstituted carbazoles as BACE1 inhibitors. *Bioorganic & Medicinal Chemistry Letters*, *27*(21), 4812–4816. https://doi.org/10.1016/j.bmcl.2017.09.058

Beukers, M. W., Wanner, M. J., Von Frijtag Drabbe Künzel, J. K., Klaasse, E. C., IJzerman, A. P., & Koomen, G. J. (2003). N6-cyclopentyl-2-(3-phenylaminocarbonyltriazene-1-yl)adenosine (TCPA), a very selective agonist with high affinity for the human adenosine A1 receptor. *Journal of Medicinal Chemistry*, *46*(8), 1492–1503. https://doi.org/10.1021/jm021074j

Choubdar, N., Golshani, M., Jalili-Baleh, L., Nadri, H., Küçükkilinç, T. T., Ayazgök, B., Moradi, A., Moghadam, F. H., Abdolahi, Z., Ameri, A., Salehian, F., Foroumadi, A., & Khoobi, M. (2019). New classes of carbazoles as potential multi-functional anti-Alzheimer's agents. *Bioorganic Chemistry*, *91*, 103164. https://doi.org/10.1016/j.bioorg.2019.103164

El-Masry, A. H. (2000). Synthesis of some new pyrimidine incorporated heterocycles for biological evaluation. *Indian Journal of Heterocyclic Chemistry*, *10*(2), 141–148.

Elif Öztürkkan Özbek, F., Uğurlu, G., Kalay, E., & Necefoğlu, H. (2020). Synthesis, characterization and computational studies of 4-[(pyridine-3-carbonyl)-hydrazonomethyl]-benzoic acid. *Journal of Molecular Structure*, *1215*, 128247. https://doi.org/10.1016/j.molstruc.2020.128247

Fang, L., Chen, M., Liu, Z., Fang, X., Gou, S., & Chen, L. (2016). Ferulic acid-carbazole hybrid compounds: Combination of cholinesterase inhibition, antioxidant and neuroprotection as multifunctional anti-Alzheimer agents. *Bioorganic & Medicinal Chemistry*, *24*(4), 886–893. https://doi.org/10.1016/j.bmc.2016.01.010

Goedert, M., & Spillantini, M. G. (2006). A century of Alzheimer's disease. *Science (New York, N.Y.)*, *314*(5800), 777–781. https://doi.org/10.1126/science.1132814

Gomes, L. M. F., Vieira, R. P., Jones, M. R., Wang, M. C. P., Dyrager, C., Souza-Fagundes, E. M., Da Silva, J. G., Storr, T., & Beraldo, H. (2014). 8-Hydroxyquinoline Schiff-base compounds as antioxidants and modulators of copper-mediated Aβ peptide aggregation. *Journal of Inorganic Biochemistry*, *139*, 106–116. https://doi.org/10.1016/j.jinorgbio.2014.04.011

Greenough, M. A., Camakaris, J., & Bush, A. I. (2013). Metal dyshomeostasis and oxidative stress in Alzheimer's disease. *Neurochemistry International*, *62*(5), 540–555. https://doi.org/10.1016/j.neuint.2012.08.014

Greig, N. H., Lahiri, D. K., & Sambamurti, K. (2002). Butyrylcholinesterase: An important new target in Alzheimer's disease therapy. *International Psychogeriatrics*, *14*(Suppl 1), 77–91. https://doi.org/10.1017/S1041610203008676

Hanif, M., Khan, I., Rama, N. H., Noreen, S., Choudhary, M. I., Jones, P. G., & Iqbal, M. (2012). Synthesis, crystal structure and b-glucuronidase inhibition activity of some new hydrazinecarboxamides and their 1,2,4-triazole derivatives. *Medicinal Chemistry Research*, *21*(11), 3885–3896. https://doi.org/10.1007/s00044-011-9929-1

Hartmann, J., Kiewert, C., Duysen, E. G., Lockridge, O., Greig, N. H., & Klein, J. (2007). Excessive hippocampal acetylcholine levels in acetylcholinesterase-deficient mice are moderated by butyrylcholinesterase activity. *Journal of Neurochemistry*, *100*(5), 1421–1429. https://doi.org/10.1111/j.1471-4159.2006.04347.x

He, Z., Qiao, H., Yang, F., Zhou, W., Gong, Y., Zhang, X., Wang, H., Zhao, B., Ma, L., Liu, H. m., & Zhao, W. (2019). Novel thiosemicarbazone derivatives containing indole fragment as potent and selective anticancer agent. *European Journal of Medicinal Chemistry*, *184*, 112–349. https://doi.org/10.1016/j.ejmech.2019. https://doi.org/10.1016/j.ejmech.2019.111764

Holzgrabe, U., Kapková, P., Alptüzün, V., Scheiber, J., & Kugelmann, E. (2007). Targeting acetylcholinesterase to treat neurodegeneration. *Expert Opinion on Therapeutic Targets*, *11*(2), 161–179. https://doi.org/10.1517/14728222.11.2.161

Jing, L., Wu, G., Kang, D., Zhou, Z., Song, Y., Liu, X., & Zhan, P. (2019). Contemporary medicinal-chemistry strategies for the discovery of selective butyrylcholinesterase inhibitors. *Drug Discovery Today*, *24*(2), 629–635. https://doi.org/10.1016/j.drudis.2018.11.012

Kanhed, A. M., Patel, D. V., Patel, N. R., Sinha, A., Thakor, P. S., Patel, K. B., Prajapati, N. K., Patel, K. V., & Yadav, M. R. (2020). Indoloquinoxaline derivatives as promising multi-functional anti-Alzheimer agents. *Journal of Biomolecular Structure and Dynamics*. https://doi.org/10.1080/07391102.2020.1840441.

Kanhed, A. M., Patel, D. V., Teli, D. M., Patel, N. R., Chhabria, M. T., & Yadav, M. R. (2020). Identification of potential Mpro inhibitors for the treatment of COVID-19 by using systematic virtual screening approach. *Molecular Diversity*, *25*(1), 383–401. https://doi.org/10.1007/s11030-020-10130-1

Kanhed, A. M., Sinha, A., Machhi, J., Tripathi, A., Parikh, Z. S., Pillai, P. P., Giridhar, R., & Yadav, M. R. (2015). Discovery of isoalloxazine derivatives as a new class of potential anti-Alzheimer agents and their synthesis. *Bioorganic Chemistry*, *61*, 7–12. https://doi.org/10.1016/j.bioorg.2015.05.005

Kedare, S. B., & Singh, R. P. (2011). Genesis and development of DPPH method of antioxidant assay. *Journal of Food Science and Technology*, *48*(4), 412–422. https://doi.org/10.1007/s13197-011-0251-1

Li, P., Shi, L., Gao, M. N., Yang, X., Xue, W., Jin, L. H., Hu, D. Y., & Song, B. A. (2015). Antibacterial activities against rice bacterial leaf blight and tomato bacterial wilt of 2-mercapto-5-substituted-1,3,4-oxadiazole/thiadiazole derivatives. *Bioorganic & Medicinal Chemistry Letters*, *25*(3), 481–484. https://doi.org/10.1016/j.bmcl.2014.12.038

Maccioni, R. B., Farías, G., Morales, I., & Navarrete, L. (2010). The revitalized tau hypothesis on Alzheimer's disease. *Archives of Medical Research*, *41*(3), 226–231. https://doi.org/10.1016/j.arcmed.2010.03.007

Makhaeva, G. F., Shevtsova, E. F., Kovaleva, N. V., Rudakova, E. V., Neganova, M. E., Dubova, L. G., Shevtsov, P. N., Aksinenko, A. Y., Sokolov, V. B., & Bachurin, S. O. (2018). Aminoadamantane conjugates with carbazole derivatives as potential multitarget agents for the treatment of Alzheimer's disease. Effect of the spacer structure. *Russian Chemical Bulletin*, *67*(11), 2121–2126. https://doi.org/10.1007/s11172-018-2338-6

Mathew, B., Baek, S. C., Parambi, D. G. T., Pil Lee, J., Joy, M., Annie Rilda, P. R., Randev, R. V., Nithyamol, P., Vijayan, V., Inasu, S. T., Mathew, G. E., Lohidakshan, K. K., Kumar Krishnan, G., & Kim, H. (2018). Selected aryl thiosemicarbazones as a new class of multi-targeted monoamine oxidase inhibitors. *MedChemComm*, *9*(11), 1871–1881. https://doi.org/10.1039/c8md00399h

Murty, M. S. R., Penthala, R., Polepalli, S., & Jain, N. (2016). Synthesis and biological evaluation of novel resveratrol-oxadiazole hybrid heterocycles as potential antiproliferative agents. *Medicinal Chemistry Research*, *25*(4), 627–643. https://doi.org/10.1007/s00044-016-1514-1

Naik, N., Vijay Kumar, H., & Swetha, H. (2010). Synthesis and evaluation of novel carbazole derivatives as free radical scavengers. *Bulgarian Chemical Communications*, *42*(1), 40–45.

Önkol, T., Gökçe, M., Orhan, İ., & Kaynak, F. (2013). Design, synthesis and evaluation of some novel 3(2H)-pyridazinone-2-yl acetohydrazides as acetylcholinesterase and butyrylcholnesterase inhibitors. *Organic Communications*, *1*, 55–67.

Oset-Gasque, M. J., & Marco-Contelles, J. (2018). Alzheimer's Disease, the "One-Molecule, One-Target" Paradigm, and the Multitarget Directed Ligand Approach. *ACS Chemical Neuroscience*, *9*(3), 401–403. https://doi.org/10.1021/acschemneuro.8b00069

Pajouhesh, H., & Lenz, G. R. (2005). Medicinal chemical properties of successful central nervous system drugs. *NeuroRx*, *2*(4), 541–553. https://doi.org/10.1602/neurorx.2.4.541

Patel, D. V., Patel, N. R., Kanhed, A. M., Patel, S. P., Sinha, A., Kansara, D. D., Mecwan, A. R., Patel, S. B., Upadhyay, P. N., Patel, K. B., Shah, D. B., Prajapati, N. K., Murumkar, P. R., Patel, K. V., & Yadav, M. R. (2019). Novel multitarget directed triazinoindole derivatives as anti-Alzheimer agents. *ACS Chemical Neuroscience*, *10*(8), 3635–3661. https://doi.org/10.1021/acschemneuro.9b00226

Patel, D. V., Patel, N. R., Kanhed, A. M., Teli, D. M., Patel, K. B., Gandhi, P. M., Patel, S. P., Chaudhary, B. N., Shah, D. B., Prajapati, N. K., Patel, K. V., & Yadav, M. R. (2020). Further studies on triazinoindoles as potential novel multitarget-directed anti-Alzheimer's agents. *ACS Chemical Neuroscience*, *11*(21), 3557–3574. https://doi.org/10.1021/acschemneuro.0c00448

Patel, D. V., Patel, N. R., Kanhed, A. M., Teli, D. M., Patel, K. B., Joshi, P. D., Patel, S. P., Gandhi, P. M., Chaudhary, B. N., Prajapati, N. K., Patel, K. V., & Yadav, M. R. (2020). Novel carbazole-stilbene hybrids as multifunctional anti-Alzheimer agents. *Bioorganic Chemistry*, *101*, 103977. https://doi.org/10.1016/j.bioorg.2020.103977

Pervez, H., Khan, N., Iqbal, J., Zaib, S., Yaqub, M., Tahir, M. N., & Naseer, M. M. (2018). Synthesis, crystal structure, molecular docking studies and bio-evaluation of some N4-benzyl-substituted isatin-3-thiosemicarbazones as urease and glycation inhibitors. *Heterocyclic Communications*, *24*(1), 51–58. https://doi.org/10.1515/hc-2017-0148

Pervez, H., Khan, N., Zaib, S., Yaqub, M., Naseer, M. M., Tahir, M. N., & Iqbal, J. (2017). Synthesis, X-ray molecular structure, biological evaluation and molecular docking studies of some N4-benzyl substituted 5-nitroisatin-3-thiosemicarbazones. *Bioorganic & Medicinal Chemistry*, *25*(3), 1022–1029. https://doi.org/10.1016/j.bmc.2016.12.012

Poljuha, D., Šola, I., Bilić, J., Dudaš, S., Bilušić, T., Markić, J., & Rusak, G. (2015). Phenolic composition, antioxidant capacity, energy content and gastrointestinal stability of Croatian wild edible plants. *European Food Research and Technology*, *241*(4), 573–585. https://doi.org/10.1007/s00217-015-2486-y

Prathima, B., Subba Rao, Y., Chalapathi, P. V., Reddy, Y. P., & Varada Reddy, A. (2012). Spectral, structural and biological analysis of Cr(III) complex with benzyloxybenzaldehyde-4-phenyl-3-thiosemicarbazone. *International Journal of Pharmacy and Pharmaceutical Sciences*, *4*(Suppl 3), 167–174.

Rydberg, P., Gloriam, D. E., & Olsen, L. (2010). The SMARTCyp cytochrome P450 metabolism prediction server. *Bioinformatics (Oxford, England)*, *26*(23), 2988–2989. https://doi.org/10.1093/bioinformatics/btq584

Rydberg, P., Gloriam, D. E., Zaretzki, J., Breneman, C., & Olsen, L. (2010). SMARTCyp: A 2D method for prediction of cytochrome P450-mediated drug metabolism. *ACS Medicinal Chemistry Letters*, *1*(3), 96–100. https://doi.org/10.1021/ml100016x

Saha, A., Kumar, R., Kumar, R., & Devakumar, C. (2010). Development and assessment of green synthesis of hydrazides. *Indian Journal of Chemistry - Section B Organic and Medicinal Chemistry*, *49*(4), 526–531.

Savelieff, M. G., Lee, S., Liu, Y., & Lim, M. H. (2013). Untangling amyloid-β, tau, and metals in Alzheimer's disease. *ACS Chemical Biology*, *8*(5), 856–865. https://doi.org/10.1021/cb400080f

Selkoe, D. J. (2003). Folding proteins in fatal ways. *Nature*, *426*(6968), 900–904. https://doi.org/10.1038/nature02264

Sens, L., De Oliveira, A. S., Mascarello, A., Brighente, I. M. C., Yunes, R. A., & Nunes, R. J. ((2018). Synthesis, antioxidant activity, acetylcholinesterase inhibition and quantum studies of thiosemicarbazones. *Journal of the Brazilian Chemical Society*, *29*(2), 343–352. https://doi.org/10.21577/0103-5053.20170146

Sinha, A., Tamboli, R. S., Seth, B., Kanhed, A. M., Tiwari, S. K., Agarwal, S., Nair, S., Giridhar, R., Chaturvedi, R. K., & Yadav, M. R. (2015). Neuroprotective role of novel triazine derivatives by activating wnt/β catenin signaling pathway in rodent models of Alzheimer's disease. *Molecular Neurobiology*, *52*(1), 638–652. https://doi.org/10.1007/s12035-014-8899-y

Sriram, D., Yogeeswari, P., Dhakla, P., Senthilkumar, P., Banerjee, D., & Manjashetty, T. H. (2009). 5-Nitrofuran-2-yl derivatives: Synthesis and inhibitory activities against growing and dormant mycobacterium species. *Bioorganic & Medicinal Chemistry Letters*, *19*(4), 1152–1154. https://doi.org/10.1016/j.bmcl.2008.12.088

Sun, L., Zhang, S. Q., & Zhong, D. F. (2004). In vitro identification of metabolites of verapamil in rat liver microsomes. *Acta Pharmacologica Sinica*, *25*(1), 121–128.

Talesa, V. N. (2001). Acetylcholinesterase in Alzheimer's disease. *Mechanisms of Ageing and Development*, *122*(16), 1961–1969. https://doi.org/10.1016/S0047-6374(01)00309-8

Thiratmatrakul, S., Yenjai, C., Waiwut, P., Vajragupta, O., Reubroycharoen, P., Tohda, M., & Boonyarat, C. (2014). Synthesis, biological evaluation and molecular modeling study of novel tacrine-carbazole hybrids as potential multifunctional agents for the treatment of Alzheimer's disease. *European Journal of Medicinal Chemistry*, *75*, 21–30. https://doi.org/10.1016/j.ejmech.2014.01.020

Veber, D. F., Johnson, S. R., Cheng, H. Y., Smith, B. R., Ward, K. W., & Kopple, K. D. (2002). Molecular properties that influence the oral bioavailability of drug candidates. *Journal of Medicinal Chemistry*, *45*(12), 2615–2623. https://doi.org/10.1021/jm020017n

Wang, T., Liu, X. h., Guan, J., Ge, S., Wu, M. B., Lin, J. P., & Yang, L. R. (2019). Advancement of multi-target drug discoveries and promising applications in the field of Alzheimer's disease. *European Journal of Medicinal Chemistry*, *169*, 200–223. https://doi.org/10.1016/j.ejmech.2019.02.076

Wang, Z., Wang, Y., Wang, B., Li, W., Huang, L., & Li, X. (2015). Design, synthesis, and evaluation of orally available clioquinol-moracin M hybrids as multitarget-directed ligands for cognitive improvement in a rat model of neurodegeneration in Alzheimer's Disease. *Journal of Medicinal Chemistry*, *58*(21), 8616–8637. https://doi.org/10.1021/acs.jmedchem.5b01222

World Alzheimer Report. (2019). *World Alzheimer Report 2019, Attitudes to dementia*. World Alzheimer Report. https://www.alz.co.uk/research/world-report-2019

Yang, W., Wong, Y., Ng, O. T. W., Bai, L. P., Kwong, D. W. J., Ke, Y., Jiang, Z. H., Li, H. W., Yung, K. K. L., & Wong, M. S. (2012). Inhibition of beta-amyloid peptide aggregation by multifunctional carbazole-based fluorophores. *Angewandte Chemie (International Ed. in English)*, *51*(8), 1804–1810. https://doi.org/10.1002/anie.201104150

Zhang, X. H., Bo-Wang, Tao, Y. Y., Ma, Q., Wang, H. J., He, Z. X., Wu, H. P., Li, Y. H., Zhao, B., Ma, L. Y., & Liu, H. M. (2020). Thiosemicarbazone-based lead optimization to discover high-efficiency and low-toxicity anti-gastric cancer agents. *European Journal of Medicinal Chemistry*, *199*, 112349. https://doi.org/10.1016/j.ejmech.2020. https://doi.org/10.1016/j.ejmech.2020.112349

Zimin, D. P., Dar'in, D. V., Rassadin, V. A., & Kukushkin, V. Y. (2018). gold-catalyzed hydrohydrazidation of terminal alkynes. *Organic Letters*, *20*(16), 4880–4884. https://doi.org/10.1021/acs.orglett.8b02019